**Atmospheric
Chemistry
and Physics
Discussions**

The global aerosol-climate model ECHAM-HAM, version 2: sensitivity to improvements in process representations

K. Zhang[1,6], D. O'Donnell[1,*], J. Kazil[2,7], P. Stier[3], S. Kinne[1], U. Lohmann[4], S. Ferrachat[4], B. Croft[5], J. Quaas[1,**], H. Wan[6], S. Rast[1], and J. Feichter[1]

[1]Max Planck Institute for Meteorology, Hamburg, Germany
[2]Cooperative Institute for Research in Environmental Sciences (CIRES), University of Colorado, Boulder, Colorado, USA
[3]University of Oxford, Oxford, UK
[4]Institute of Atmospheric and Climate Science, ETH Zürich, Switzerland
[5]Department of Physics and Atmospheric Science, Dalhousie University, Halifax, Canada
[6]Pacific Northwest National Laboratory, Richland, WA, USA
[7]NOAA Earth System Research Laboratory (ESRL), Boulder, Colorado, USA
[*]now at: Finnish Meteorological Institute, Helsinki, Finland
[**]now at: University of Leipzig, Leipzig, Germany

Correspondence to: K. Zhang (kai.zhang@pnnl.gov)

ACPD

12, 7545–7615, 2012

Aerosol properties in ECHAM-HAM2

K. Zhang et al.

Title Page

Abstract	Introduction
Conclusions	References
Tables	Figures

|◄ | ►|

◄ | ►

Back | Close

Full Screen / Esc

Printer-friendly Version

Interactive Discussion

Title Page

Abstract | Introduction

Conclusions | References

Tables | Figures

◄ | ►

◄ | ►

Back | Close

Full Screen / Esc

Printer-friendly Version

Interactive Discussion

Abstract

This paper introduces and evaluates the second version of the global aerosol-climate model ECHAM-HAM. Major changes have been brought into the model, including new parameterizations for aerosol nucleation and water uptake, an explicit treatment of sec-

5 ondary organic aerosols, modified emission calculations for sea salt and mineral dust, the coupling of aerosol microphysics to a two-moment stratiform cloud microphysics scheme, and alternative wet scavenging parameterizations. These revisions extend the model's capability to represent details of the aerosol lifecycle and its interaction with climate.

10 Sensitivity experiments are carried out to analyse the effects of these improvements in the process representation on the simulated aerosol properties and global distribution. The new parameterizations that have largest impact on the global mean aerosol optical depth and radiative effects turn out to be the water uptake scheme and cloud microphysics. The former leads to a significant decrease of aerosol water contents in the

15 lower troposphere, and consequently smaller optical depth; the latter results in higher aerosol loading and longer lifetime due to weaker in-cloud scavenging.

The combined effects of the new/updated parameterizations are demonstrated by comparing the new model results with those from the earlier version, and against observations. Model simulations are evaluated in terms of aerosol number concentrations

20 against measurements collected from twenty field campaigns as well as from fixed measurement sites, and in terms of optical properties against the AERONET measurements. Results indicate a general improvement with respect to the earlier version. The aerosol size distribution and spatial-temporal variance simulated by HAM2 are in better agreement with the observations. Biases in the earlier model version in aerosol

25 optical depth and in the Ångström parameter have been reduced. The paper also points out the remaining model deficiencies that need to be addressed in the future.

Aerosol properties in ECHAM-HAM2

K. Zhang et al.

1 Introduction

Although it is widely believed that natural and anthropogenic aerosols play an important role in determining the current state and future changes of the Earth's climate, some physical processes in the aerosol lifecycle are not yet understood with certainty.
Quantifications of the climatic effects of aerosols, particularly through their impacts on clouds, remain insufficient. Numerical models, together with observational data from a variety of sources, provide a powerful tool for advancing our understanding of the complex interactions between aerosols and climate. Lessons learnt from earlier studies using simple bulk methods (e.g., Langner and Rodhe, 1991; Feichter et al., 1996) gradually led to appreciation of the importance of microphysics in aerosol modelling. The newer models have thus included more detailed descriptions of aerosol composition and size distribution, using different approaches (Wilson et al., 2001; Jacobson, 2001; Vignati et al., 2004; Easter et al., 2004; Stier et al., 2005; Spracklen et al., 2005; Liu et al., 2005; Bauer et al., 2008; Liu et al., 2011).

The ECHAM5-HAM model (Stier et al., 2005) developed at the Max Planck Institute for Meteorology was one of the earlier examples of a global atmospheric general circulation model that can dynamically predict the composition and size distribution of aerosols by taking into account the most important chemical and physical processes from the micro- to the global scale, and in return, calculate the radiative effects of aerosols on the atmospheric dynamics. In addition to the evaluation presented by Stier et al. (2005), the model has been compared with other models and with observations through participation in the AeroCom (Aerosol Comparisons between Observations and Models) model inter-comparison project (http://aerocom.met.no) and the EUCAARI (European Integrated project on Aerosol Cloud Climate and Air Quality interactions) model inter-comparison (Kulmala et al., 2011). The simulated aerosol mass budget, residence time, and optical properties are within the ranges of multi-model spread (Textor et al., 2006, 2007; Kinne et al., 2006). The estimated direct forcing of aerosols is close to the multi-model mean (Schulz et al., 2006).

Since first released in 2005, the model has been widely used in process studies (e.g., Hoose et al., 2008; Croft et al., 2009; Makkonen et al., 2009) and for investigations in the climate impact of aerosols (e.g., Roeckner et al., 2006b; Stier et al., 2006; Kloster et al., 2008; Lohmann and Hoose, 2009; Fischer-Bruns et al., 2010; Folini and Wild, 2011; Kazil et al., 2012). The first released version, designed with a focus on tropospheric aerosols, has been extended into the stratosphere and used in volcanic eruption and geo-engineering studies (e.g., Niemeier et al., 2009; Timmreck et al., 2010; Niemeier et al., 2011). Apart from being coupled with ECHAM5 (Roeckner et al., 2003, 2006a), the complete aerosol module HAM, or substantial parts of it, has been implemented in several other model systems, for example by Mashayekhi et al. (2009), Pringle et al. (2010), Zhang et al. (2010), and Bergman et al. (2011).

In the past years, through further evaluation as well as various applications, several biases in ECHAM-HAM have been brought to attention. For example, the evaluation of the simulated aerosol absorption revealed negative biases (Stier et al., 2007). The Aitken mode particle number concentration is underestimated in the lower troposphere over the industrial regions compared to aircraft measurements (Stier et al., 2005), and so is the accumulation mode number concentration over the ocean, according to ship measurements (Hoose et al., 2008). The simulated aerosol optical depth (AOD) and extinction profiles has a systematic negative bias in high-latitude regions (Koch et al., 2009; Bourgeois and Bey, 2011) and positive bias over the open oceans (Croft et al., 2009). The Angström parameter over the ocean is on the large large side compared to the Moderate Resolution Imaging Spectroradiometer (MODIS) satellite retrieval. These issues, together with the simplifications made for secondary organic aerosols (SOA) and the lack of physically-based coupling between aerosols and clouds, motivated the further improvement of ECHAM-HAM.

A series of attempts have been made to identify the sources of these errors and to improve model performance. The refractive index for black carbon has been updated to reduce the negative bias of absorption aerosol optical depth (Stier et al., 2007). The four-band shortwave radiative transfer scheme in the atmospheric model

has been extended with two additional bands (Cagnazzo et al., 2007). A newer aerosol nucleation parameterization has been adopted, and additional mechanisms included (Kazil et al., 2010). A more detailed and explicit treatment of SOA was implemented (O'Donnell et al., 2011), as well as a new scheme for calculating the hygroscopic growth of aerosol particles. The wet scavenging schemes have been updated (Croft et al., 2009, and this work). A two-moment cloud microphysics scheme is implemented and coupled with aerosol microphysics (Lohmann et al., 2007). The on-line calculation of dust and sea salt emissions have also been modified (Cheng et al., 2008, and this work). A satellite simulator (Quaas et al., 2004, see also http://www.euclipse.eu/downloads/D1.2_euclipse_modissimulator.pdf) is implemented in the model which diagnoses cloud quantities consistently with passive satellite retrievals as from the MODIS instrument, and samples the spatial and temporal incidences of the overpasses of polar-orbiting satellites. This facilitates the comparison between model results and the observations from spaceborne instruments. These revisions have brought us to the point where a second version of this aerosol-climate model is ready for release. This new version, referred to as ECHAM-HAM2 (or simply HAM2), participated in phase II of the AeroCom model inter-comparison (Schulz et al., 2009).

The main objective of the present paper is to analyse and quantify the effects of improvements in the process representation on the simulated aerosol properties, global distribtion, and radiative effects. Although some of the new features have already been discussed in the publications cited above, the authors therein mainly concentrated on specific schemes for individual processes. The model evaluation was often limited to aspects most closely related to the process in question. Furthermore, some of the above-cited studies with ECHAM-HAM were based on intermediate (unreleased) code versions that included incremental changes in model configuration. As the aerosol processes and their interactions with each other and with model meteorology are often nonlinear, it is not always easy to draw conclusions on the effect of a particular modification by inter-comparing results reported in these publications. An important part of the present paper is a series of sensitivity simulations that are all performed with the

Aerosol properties in ECHAM-HAM2

K. Zhang et al.

"official" HAM2 as reference, and with a single aspect of the model updates reverted to the HAM1 configuration (see Sect. 4). In this way we attempt to provide a clean evaluation of the impact of each individual modification. The combined effects are analyzed in Sect. 5 in the comparison of HAM2 simulations with those from the previous version, as well as against observation. Before showing these results, we provide a summary of the basic features of the HAM model in Sect. 2, and describe the simulation design in Sect. 3. Conclusions drawn from this work are presented in Sect. 6. As in the paper by Stier et al. (2005), we concentrate our analysis on aerosols in the troposphere. There are some addtional model updates related to stratospheric aerosols which have not yet been included in the code used in this study. These developments were presented in Niemeier et al. (2009).

2   Model overview

The aerosol module HAM (Stier et al., 2005), coupled to the global climate model ECHAM5 (Roeckner et al., 2003, 2006a), predicts the evolution of an aerosol ensemble with five internally and externally mixed compositions: sulfate (SU), black carbon (BC), particulate organic matter (POM), sea salt (SS), and mineral dust (DU). The size distribution of this aerosol population is described by seven log-normal modes with prescribed variance in the M7 aerosol module (Vignati et al., 2004). The prognostic variables are the particle number concentration of each mode, as well as the mass concentration of each compound present in that mode.

The emissions of sea salt and dust are computed interactively (Tegen et al., 2002; Guelle et al., 2001; Stier et al., 2005). Those of sulfur dioxide (SO_2) and particulate sulfate, black carbon and primary organic aerosols (POA) are prescribed following the specifications of AeroCom. Natural emissions of dimethyl sulfide (DMS) from the marine biosphere are calculated online (Kloster et al., 2006). Terrestial DMS emissions are prescribed according to Pham et al. (1995).

The sulfur chemistry module is based on the work by Feichter et al. (1996). Prognostic variables include concentrations of DMS, SO_2 and gas- and aqueous-phase sulfate. Oxidant fields, including hydroxyl radical (OH), hydrogen peroxide (H_2O_2), nitrogen dioxide (NO_2), and ozone (O_3), are prescribed using three-dimensional monthly mean model output for present-day condition from the MOZART model (Horowitz et al., 2003). Sulfuric acid gas produced from gas-phase chemistry can either condense on existing aerosol particles or nucleate to form new particles. Sulfate produced from aqueous phase chemistry is distributed to pre-existing soluble accumulation mode and coarse mode aerosol particles.

The aerosol microphysics sub-module M7 of Vignati et al. (2004) simulates the formation and growth of aerosol particles due to nucleation and condensation of sulfuric acid gas, the coagulation of particles, and aerosol water uptake. These processes lead to re-distribution of particle number and mass among different modes. Sink processes, namely dry deposition, sedimentation and wet deposition, are parameterized as functions of the aerosol size distribution, composition, and mixing state, as well as the meteorological conditions.

Radiative properties of aerosols are dynamically computed based on their chemical composition (including the water content) and particle size using a pre-calculated look-up table established using the Mie theory.

Further details of the features mentioned above are described in Stier et al. (2005) and the references therein. These remain unchanged through all model versions that exist so far. In the following parts of this paper, when mentioning these features, or our model development effort in general, we will use the term "ECHAM-HAM" (or simply "HAM"). When it is necessary to distinguish, "HAM1" will be used to refer to the specific model configuration described by Stier et al. (2005), and "HAM2" for the new version presented here. Table 1 provides an overview of the updates in HAM2 with respect to HAM1. Further details and the impacts on aerosol simulation are discussed in Sect. 4. To facilitate discussions in the following sections and for the convenience of the readers,

the diagram in Fig. 1 presents the modal structure of the aerosol population in our model.

3 Simulation setup

We performed simulations of the year 2000 forced by sea surface temperature/sea ice prescriptions of the same year from the Second Atmospheric Model Intercomparison Project (http://www-pcmdi.llnl.gov/projects/amip/). Emissions of anthropogenic aerosols and their precursors, as well as biomass burning and volcanic aerosols are prescibed according to AeroCom Phase I emission data for the year 2000 (Dentener et al., 2006). Each integration starts from a meteorological state that is routinely used in climate simulations with ECHAM5. The initial concentrations of all aerosols and prognostic precursors are zero. Three months of integration are performed prior to January 2000 in each simulation. This is considered as the spin-up phase and not included in the analysis presented later in the paper.

Since the purpose of this study is to evaluate the aerosol module HAM rather than the host model ECHAM5, we carry out nudged simulations, which relax the meteorological fields towards the ERA-40 reanalysis (Uppala et al., 2005). This allows for detailed comparison between model results and observations, and also reduces the length of simulation that is required to draw sound conclusions. The responses of model results to formulation/configuration changes in the following sections are significant in magnitude, and are consistently seen in different diagnostics.

To evaluate the aerosol properties in HAM2 and their differences compared to the earlier version HAM1, integrations are performed using the corresponding default model configurations. In addition, a number of sensitivity simulations are carried out and are discussed in Sect. 4. In each simulation, one component of the parameterized sub-grid processes in HAM2 is reverted to the old HAM1 setup, or replaced by an alternative that is implemented in the new version but not yet set as default. A list of simulations carried out in this study is given in Table 2.

Full Screen / Esc

Printer-friendly Version

Interactive Discussion

4 Model updates and their effects

In this section we describe the model updates with respect to HAM1, and discuss their impact on the simulated aerosol distributions and properties.

4.1 Sulfuric acid gas and aerosol nucleation

The conversion of sulfuric acid (H_2SO_4) gas to aerosol particles is one of the major mechanisms of particle formation in the atmosphere. In the HAM model sulfuric acid gas is produced by the oxidation of SO_2, and removed by nucleation as well as condensation onto already existing aerosol particles. The strength of nucleation in the model is not only determined by the nucleation mechanism, but also strongly affected by the abundance of H_2SO_4 gas and the balance between its source and sink terms.

Nucleation of H_2SO_4/H_2O in the earlier model version was desribed with the scheme of Vehkamäki et al. (2002) or that of Kulmala et al. (1998). The former was the default choice because it is based on a thermodynamically consistent version of the classical binary homogeneous nucleation theory, and is valid for a broader range of thermodynamical conditions (cf. Table 3). Kazil et al. (2010) implemented the scheme of Kazil and Lovejoy (2007) for neutral and charged nucleation of H_2SO_4 and H_2O. This parameterization is based on laboratory measurements using a semi-analytical approach to calculate aerosol formation rates. It is now the default nucleation scheme in HAM2. In the planetary boundary layer, HAM2 also considers the nucleation of H_2SO_4 and an organic compound via cluster activation (Kulmala et al., 2006; Riipinen et al., 2007), and kinetic nucleation (Laakso et al., 2004; Kuang et al., 2008), although these processes are intentionally limited to forested areas. In the standard model configuration, these nucleation pathways are switched off.

Another major change between HAM1 and HAM2 is the treatment of sulfuric acid gas. In the model, production and condensation are linear processes from the point of view of the gas-phase H_2SO_4 equation (cf. Eq. (2) in Vignati et al., 2004), while nucleation is a nonlinear process. In the default HAM1 configuration the gas-phase

H_2SO_4 equation was numerically solved in three consecutive steps, each taking care of one process and using explicit time integration to update the H_2SO_4 concentration for the next step. Kokkola et al. (2009) proposed a different operator-splitting algorithm in which the production-condensation equation is solved analytically in the first step to provide an intermediate estimate of sulfuric acid gas concentration, followed by a second step accounting for nucleation. This new algorithm has the advantage of converging towards the exact solution of the production-condensation equation when nucleation is weak. Kokkola et al. (2009) showed with a box model that this scheme outperformed the original algorithm. In addition to the revised numerics, Kazil et al. (2010) introduced the assumption that in the cloudy portion of a grid box, all H_2SO_4 gas condenses on the largest soluble particles if there is any, and on the largest insoluble particles otherwise. There is complete removal of sulfuric acid gas in clouds, and no aerosol nucleation takes place within them.

To demonstrate the impact of these changes at the global scale, we present vertical cross-sections of the number concentration of ultra-fine (nucleation mode) particles together with the mass concentration of H_2SO_4 gas in Fig. 2. The right column shows results from the standard HAM2 configuration; The middle column uses the Kazil et al. (2010) (HAM2 default) nucleation parameterization but the old time stepping method and without complete in-cloud removal (referred to as experiment HAM2_H2SO4 in Table 2). The left column, corresponding to experiment HAM2_NUL, uses the HAM1 set-up which includes the Vehkamäki et al. (2002) parameterization, three-step explicit numerics, and no distinction between condensation in clouds and in the cloud-free parts. All other aspects are identical in the three simulations.

Switching from Vehkamäki et al. (2002) to the Kazil and Lovejoy (2007) parameterization leads to an upward shift of the highest concentrations of fine particles (Fig. 2a–b), due to a strong reduction of nucleation at altitudes of 400–150 hPa and a moderate increase at 150–50 hPa (not shown). Accordingly, there is more sulfuric acid gas remaining in the air in the upper troposphere, and less near the tropical tropopause (Fig. 2d–e). Changing the handling of the H_2SO_4 gas equation, on the other hand,

results in higher concentrations for the nucleation mode particle number, and a qualitative change in the vertical distribution of the sulfuric acid gas. To understand these results, it is worth noting that in HAM1 the H_2SO_4 concentration seen by the condensation calculation is the value updated after taking into account *only* the chemical production. Because of the large time step used in the climate model, this intermediate concentration has a large positive bias when production is strong. The subsequently computed condensation rate is thus significantly overestimated. This explains the box model results presented in Fig. 1 of Kokkola et al. (2009) in which the "M7 original" scheme systematically underestimates the sulfuric acid gas concentrations in all three scenarios investigated therein. We have carried out a sensitivity experiment similar to HAM2_H2SO4, in which the first two steps (production and condensation) in the old time integration scheme are solved together using a simple Euler forward (explicit) scheme. The effect is a clear increase of the H_2SO_4 concentration in comparison to Fig. 2d–e. In particular, in the near-surface layers, the magnitudes and characteristic pattern become very similar to Fig. 2f (not shown). An additional simulation reveals that the differences between panels e and f in the tropical upper troposphere and above the Southern Hemisphere storm track are caused by the distinction between cloud-free and in-cloud condensation of the H_2SO_4 gas in HAM2 (not shown).

Sensitivity experiments have also been performed regarding nucleation in the boundary layer (HAM2_cluster and HAM2_kinetic in Table 2). These results are discussed in Sects. 5.2 and 5.3 in the context of comparison with observations.

4.2 Secondary organic aerosol (SOA)

The first version of HAM had a very simple treatment of secondary organic aerosols following the AeroCom approach (Dentener et al., 2006). 15 % of the prescribed natural terpene emission was oxidized in the surface layer and condensed immediately on existing aerosol particles (Stier et al., 2005; Kanakidou et al., 2005). The SOA therein was assumed to have identical properties to primary organic aerosols (POA).

Title Page

Abstract | Introduction

Conclusions | References

Tables | Figures

|◄ | ►|

◄ | ►

Back | Close

Full Screen / Esc

Printer-friendly Version

Interactive Discussion

O'Donnell et al. (2011) implemented an explicit SOA module in ECHAM-HAM, which handles aerosols originating from biogenic (isoprene and monoterpenes) and anthropogenic (xylene, toluene and benzene) sources. The emissions of biogenic precursors are computed interactively, while those of the anthropogenic precursors are prescribed. Transport and oxidation processes of the precursors, as well as the partitioning of semivolatile oxidation products into gas and aerosol phases, are explicitly described. The two-product model of Odum et al. (1996) is used for biogenic SOA formation, meaning that each biogenic precursor has two oxidation products of different volatility. Anthropogenic oxidation products can be lumped together (by changing model configuration via namelist). SOA formed from anthropogenic sources are assumed as non-volatile following the work of Ng et al. (2007). The five SOA products (four from biogenic sources, one from anthropogenic sources) are assumed to be absorbed by POA and by each other, thus the modes in which SOA can occur are the same as those that contain POA, namely the Aitken insoluble, Aitken soluble, accumulation soluble, and coarse soluble modes (cf. Fig. 1). Refractive indices of SOA are assumed the same as those of POA. Further details are given by O'Donnell et al. (2011).

When the new SOA scheme is switched on, the interactively computed biogenic precursor emissions ($441.6\,\text{Tg yr}^{-1}$ isoprene and $86.3\,\text{Tg yr}^{-1}$ monoterpenes) produce about $119.1\,\text{Tg yr}^{-1}$ semi-volatile condensable species ($106.5\,\text{Tg yr}^{-1}$ from isoprene, $12.6\,\text{Tg yr}^{-1}$ from monoterpenes). These oxidation products form 15.7 Tg SOA per year, which, in terms of absolute value, is not far away from the old scheme ($19.1\,\text{Tg yr}^{-1}$, Dentener et al., 2006). The SOA yield, however, is only 3 % and much smaller than specified by AeroCom (15 %). This reflects the dominance of isoprene emissions, which were not included in the old scheme. The anthropogenic emissions result in $5.5\,\text{Tg yr}^{-1}$ oxidation products, which are assumed non-volatile and convert totally to SOA.

The spatial distribution of aerosol concentrations also changes substantially. In Fig. 3 we present zonal mean mass concentration of total organic aerosols (also referred to as particulate organic matter, POM) simulated by HAM2 with different SOA schemes. The

most evident effect of the new scheme is the higher loading in the upper troposphere, associated with enhanced SOA formation due to tropical convective transport of the condensable oxidation products, especially high-volatility products associated with isoprene oxidation, which condense only at very low temperatures. Results obtained with the original SOA scheme (Fig. 3a), in contrast, resembles closely the POA distribution of HAM1 (see Fig. 5 of O'Donnell et al., 2011), as one would expect. The differences in the lower troposphere in Fig. 3c mainly reflect the changes in precursor emissions. The increased concentrations between 20° S and 15° N are connected to the biogenic sources, while those at 15–40° N are primarily related to the anthropogenic sources.

4.3 Water uptake

Water uptake is an important process that changes the size and optical properties of aerosol particles. In the real world non-organic aerosols that contain sulfate and/or sea salt, and some organic aerosols, are hygroscopic. In HAM1, however, water uptake was considered only for non-organic particles. For pure sulfate particles, water uptake was calculated using regression fits to solutions of the generalized Kelvin equation (Zeleznik, 1991); For mixed particles that contain sulfate but no sea salt, sulfate mass was regarded as the effective soluble mass and used in the calculation of the equilibrium particle density; for particles containing sea salt, complete ion dissociation was assumed, with the water uptake calculated according to the ZSR method (Zdanovskii, 1948; Stokes and Robinson, 1966), which regards an aerosol particle as a solution of mixed electrolytes.

When introducing the new SOA scheme mentioned in the previous subsection, O'Donnell et al. (2011) implemented a semi-empirical water uptake scheme based on the κ-Köhler theory (Petters and Kreidenweis, 2007), now used for all hygroscopic aerosols in HAM2. This approach uses a prescribed hygroscopicity parameter κ for each substance (Table 4). For an internally-mixed aerosol particle, the overall κ value is calculated by taking the volume-weighted sum of the parameter of each soluble compound. Having computed the hygroscopicity parameter of a particle, and with its

dry diameter, the air temperature and relative humidity known, the growth factor of particle radius can be determined using Eq. (11) of Petters and Kreidenweis (2007) and therefore the aerosol water content. In the model, a look-up table is used to enhance computational efficiency.

The new scheme results in a significant decrease in water uptake in the lower troposphere and a slight increase aloft, reducing the total aerosol water from 75 Tg (HAM1) to 51 Tg (HAM2), the latter being closer to the multi-model average of the AeroCom Project (35 Tg, Textor et al., 2006). The absolute and relative contributions of aerosol water to aerosol optical depth (AOD) decrease from 0.105 and 74.8 % (HAM1) to 0.094 and 69.8 % (HAM2), respectively.

4.4 Sea salt emission

Sea salt emission is a primary source of soluble accumulation mode and coarse mode aerosol over the oceans in the model. The emission fluxes are parameterized as functions of 10-m wind speed following the work of Monahan et al. (1986) and Smith and Harrison (1998). In HAM1, look-up tables of emission flux against 10-m wind were established using the Monahan formula for small particles (dry radius $r < 2\,\mu m$), the Smith-Harrison formula for large particles ($r > 4\,\mu m$), and a smoothly merged function for the size range in between (Stier et al., 2005). Zhang et al. (2010) noticed that the partitioning of sea salt emission between accumulation and coarse modes in ECHAM-HAM1 was evidently different from two other models using the same microphysics package, and attributed the differences to the emission scheme.

In HAM2 we still use the source functions of Monahan et al. (1986) and Smith and Harrison (1998), but directly apply the Monahan et al. (1986) formula for the radius range of 2–4 μm without merging, and replace the look-up tables by online integration of the source functions. As shown in Fig. 4, the new implementation produces stronger emissions in the accumulation mode and weaker in the coarse mode in terms of number flux. The ratio of the accumulation mode number flux to that of the coarse mode is now 7.7 in contrast to 1.6 in HAM1, and is closer to the value 6.7 that can be derived

from the Dentener et al. (2006) emission dataset recommended for AeroCom. In terms of mass flux, there is an increase of emission in both modes (not shown), implying that the emitted coarse mode particles are larger than in HAM1. Further discussions of these changes are presented in Sect. 5.

4.5 Dust emission

Dust emissions in HAM1 were calculated interactively using the scheme of Tegen et al. (2002) which was based on observations from Africa but resulted in considerable biases in East Asia. Cheng et al. (2008) made attempts to improve dust emission by modifying the surface conditions used in the model. They employed a new global dataset of aerodynamic roughness length derived by Prigent et al. (2005) from satellite retrievals, and the East-Asian soil properties from Laurent et al. (2006). In addition, impact of soil moisture was taken into account when computing the threshold frictional wind velocity of dust mobilization. Because the satellite-derived roughness lengths were much larger than those used in the original model, a scaling factor had to be applied to the frictional velocity and fine-tuned in order to give a reasonable global total emission. Recent model evaluation has revealed that this modification leads to an overestimate of AOD over North Africa, while the inclusion of soil moisture in frictional velocity calculation does not lead to significant improvement (not shown). Therefore in HAM2 only the modification of East Asia soil properties is adopted from the work of Cheng et al. (2008).

To demonstrate the effect of this update, the standard HAM2 results are compared with a sensitivity simulation HAM2_DU performed using the old soil property data. The characteristic spatial pattern of dust emission is largely unchanged, but the strength increases by a factor of about 4 (Fig. 5a). The simulated near surface dust concentration (Fig. 5b) and AOD (Fig. 5c) in the vicinity of the source regions as well as in the downstream areas also increase, which leads to better agreements between model and observation (not shown).

4.6 Aerosol wet deposition

The removal of aerosol species from the atmosphere by precipitation happens through processes that occur both in and below clouds.

For in-cloud scavenging, the removal rates in our model are a function of a scavenging parameter R defined as the fraction of the aerosol mass or number concentration that is considered to be contained in the cloud-droplets or ice-crystals in the cloudy part of the grid box.

In HAM1 a constant in-cloud R was prescribed for each aerosol mode and cloud type (see Table 3 in Stier et al., 2005). In reality, the partitioning of aerosols between those contained in cloud-droplets or ice-crystals as opposed to outside of these hydrometeors depends on details of the particle characteristics (e.g., chemical composition) and environmental conditions (e.g., temperature and updraft velocity). For mixed-phase clouds, Verheggen et al. (2007) analyzed measurements obtained at the high alpine research station Jungfraujoch (Switzerland), and derived the following relationship between air temperature (T, in Kelvin) and the fraction of aerosols (F_N) contained in the cloud droplets or ice crystals:

$$F_N(T) = 0.031 + 0.93 \left[1 + \exp(-\frac{T - 269.51}{3.42}) \right]^{-1} \tag{1}$$

Using this formula, we have added in HAM2 a new option for the scavenging parameter of mixed-phase stratiform clouds:

$$R_{\text{mix},i}(T) = \frac{F_N(T)}{F_N(T_0)} R_{0,i}, \tag{2}$$

where $T_0 = 273.15\,\text{K}$; $R_{0,i}$ is the scavenging parameter for aerosol mode i in mixed-phase clouds as prescribed by Stier et al. (2005). The scaled scavenging parameters $R_{\text{mix},i}$ decrease with temperature, and are generally smaller than the original values. Consequently wet deposition becomes weaker and aerosol loading larger, especially

in middle and high latitude regions, as can been seen from the annual mean AOD (Fig. 6a). The relative changes are larger in the regions from 45° N/45° S poleward since the total aerosol loading is considerably smaller in the high latitudes than in the tropics (cf. Fig. 15a). The weakening of in-cloud scavenging is potentially beneficial for reducing model error since HAM1 underestimated aerosol mass concentrations in high latitude regions.

Below-cloud scavenging by rain and snow are considered separately in HAM. Mode-dependent impaction scavenging coefficients were prescribed in HAM1 for rain. For the impaction scavenging by snow, a fixed coefficient of $0.005\,\mathrm{m}^2\,\mathrm{kg}^{-1}$ was used for all modes (Stier et al., 2005). This simple treatment has been updated by Croft et al. (2009) to take into account aerosol and collector size distributions in the rain case, and aerosol size in case of snow. These changes yield a reduction of AOD at most geographical locations (Fig. 6b, corresponding to a 8 % decrease in global mean), es-pecially over the storm tracks, and in mid-latitude continental areas that are associated with high aerosol concentrations.

The combined effect of modified in-cloud and below-cloud scavenging is shown by the bottom panel of Fig. 6. AOD reductions occur close to East Asian source regions and Southern Hemisphere storm track regions, while AOD increases are primarily at the high latitudes. However, this is not a simple addition of panels a and b, because in-cloud and below-cloud removal happen at different vertical levels. Various other factors, including aerosol source, horizontal and vertical transport timescale and pathway, are also relevant in determining the combined effect shown in Fig. 6c.

To the model users we point out that the updates described in this subsection are available in HAM2 but not switched on as default. A comprehensive evaluation of their impacts on model climatology is planned for future code release.

4.7 Cloud microphysics and its coupling with aerosols

In the earlier model ECHAM-HAM1 the stratiform cloud microphysics scheme (Lohmann and Roeckner, 1996) predicted mass concentrations of water vapor, cloud

Title Page

Abstract | Introduction

Conclusions | References

Tables | Figures

◄ | ►|

◄ | ►

Back | Close

Full Screen / Esc

Printer-friendly Version

Interactive Discussion

water and cloud ice by taking into account phase transitions, precipitation processes (autoconversion, accretion, aggregation), evaporation of rain and melting of snow, as well as sedimentation of cloud ice. Regarding stratiform cloud formation, the cloud droplet number concentrations (CDNC) were prescribed as functions of pressure and surface type (land or ocean). The conversion of aerosol particles into cloud droplets – often referred to as aerosol activation or cloud droplet nucleation – was not considered. While clouds could directly affect the aerosol population via wet scavenging, aerosols could only affect clouds via the direct and semi-direct aerosol effects on model meteorology.

In order to explicitly simulate the effects of aerosols on stratiform cloud microphysics, Lohmann et al. (2007) introduced a two-moment scheme, with further improvements proposed by and Lohmann and Hoose (2009). The new scheme includes prognostic equations for number concentrations of cloud droplets and ice crystals, and is used as the default stratiform cloud microphysics scheme for HAM2. Many details of the parameterized phase change and precipitation processes (e.g. autoconversion and accretion) are different from the work of Lohmann and Roeckner (1996). The coupling between aerosols and cloud microphysics is implemented as follows: aerosol activation in warm clouds is described by the semi-empirical scheme of Lin and Leaitch (1997). Autoconversion of cloud droplets to rain is parameterized as in Khairoutdinov and Kogan (2000). Homogeneous ice nucleation in cirrus clouds is assumed to happen at air temperatures below $-38\,^\circ$C when supercooled solution droplets freeze. The production rate of ice crystals is computed following Kärcher and Lohmann (2003). Heterogenous nucleation happens in the model when dust exists and the air temperature lies between $-38\,^\circ$C and $0\,^\circ$C. Internally mixed dust and black carbon aerosols are assumed to act as immersion nuclei while only externally mixed dust particles act as contact nuclei. Contact freezing by black carbon is not considered as it is quite uncertain (Lohmann and Hoose, 2009).

In Fig. 7a–b we present the annual mean shortwave cloud radiative forcing simulated with the standard ECHAM-HAM2 model, as well as the differences from a

Full Screen / Esc

Printer-friendly Version

Interactive Discussion

sensitivity experiment HAM2_CLD that uses the old stratiform cloud microphysics scheme (Lohmann and Roeckner, 1996) without prognostic CDNC. One can see a clear reduction in cloud forcing in the marine stratocumulus regions, and increase in the Southern Hemisphere storm track, caused predominantly by changes in the cloud liquid water path (Fig. 7c). Over the North Atlantic and North Pacific, this effect is largely counteracted by larger droplet sizes resulting from the fact that in these (cleaner) areas the updated model predicts smaller CDNC than prescribed by the old model (not shown). In terms of global mean, the liquid water path of the HAM2_CLD and HAM2 simulations are $50\,\mathrm{g\,m^{-2}}$ and $85\,\mathrm{g\,m^{-2}}$, respectively. In contrast, the increase in global mean precipitation rate is only marginal ($<2\,\%$). It follows that the autoconversion rate in the new cloud scheme is considerably smaller, which has direct consequences for the in-cloud scavenging of aerosols. Note that the parameters controlling the autoconversion rate, as in all climate models, are affected by the general model tuning (see, e.g., Lohmann and Ferrachat, 2010). Further discussion in this aspect can be found in Sect. 5.1.

As a side remark we point out that the particle size effect on aerosol activation is highly simplified in the parameterization by Lin and Leaitch (1997). The Köhler theory based activation scheme by Abdul-Razzak and Ghan (2000) has been implementd into HAM2, and is evaluated in Stier et al. (2012).

5 Evaluation of HAM2 against HAM1 and observations

Having documented in the previous section the new features in model formulation and their individual impacts on simulation results, we now move on to their combined effects. This section compares the overall behavior of HAM2 with that of the earlier version HAM1, and when possible, against observations.

5.1 Global mean aerosol mass budgets and concentrations

We start the intercomparison with the annual mean global mass budget of different aerosol types shown in Table 5. Results from the AeroCom intercomparison project (Dentener et al., 2006) are also included in the table, so as to place our results in perspective.

To the first order, HAM1 and HAM2 have very similar mass budgets. The relative differences are, in most cases, considerably smaller than the discrepencies among the AeroCom models. On the other hand, differences can still be clearly seen between the two HAM versions. For instance the nucleation source of sulfate aerosol increases considerably in the new version (Table 5, first block), which is in agreement with earlier discussions in Sect. 4.1. HAM2 also shows a marked increase (+49 %) in POM burden, which is not surprising considering the inclusion of the explicit SOA module.

Another point worth noting is the shorter lifetime of sea salt in HAM2 (Table 5, fourth block). In Sect. 4.4 we mentioned that the modified emission scheme produces stronger *number* fluxes in the accumulation mode and weaker in the coarse mode, as well as an increase of mass flux in both modes compared to HAM1. Consequently, the coarse mode particles become much larger than in HAM1, and are more efficiently removed from the atmosphere through dry deposition and sedimentation. Because coarse mode particles constitute more than 95 % of the total sea salt mass, they play a determining role in the changes in sea salt sinks we see in Table 5.

The four aerosol species other than sea salt have longer lifetimes in HAM2 compared to HAM1 (Table 5). This is mainly related to cloud microphysics and wet deposition. In Table 6 the two simulations HAM2 and HAM2_CLD are compared, which differ only in cloud microphysics in terms of model configuration. The new cloud scheme leads to an increase of lifetime, especially for the soluble species (sulfate, sea salt and SOA), due to weaker in-cloud scavenging.

In Fig. 8 we present the annual and zonal mean mass concentration of the five aerosol types. Consistent with Table 5, an overall increase in aerosol burden can be

seen in the right column, occuring mainly in the free troposphere. This is particularly true for POM which, as already pointed out in Sect. 4.2, results from the vertical transport of condensable gases and the SOA formation associated with tropical convection. The near-surface layers feature marginal changes within a factor of 1.5 (except in the Polar Regions). A comparision of the simulated monthly mean surface mass concentrations against the EMEP (European Monitoring and Evaluation Programme), IMPROVE (Interagency Monitoring of Protected Visual Environments) and the University of Miami networks is presented in Fig. A1. The results are very similar to Fig. 3 in Stier et al. (2005), thus are not discussed futher in this paper.

5.2 Condensation nuclei

This subsection evaluates the simulated number concentrations of condensation nuclei (CN, i.e. aerosol particles of dry diameter larger than 0.01 µm) using a collection of aircraft measurements between the years 1991 and 2008 obtained from the Langley Research Center of National Aeronautics and Space Administration (NASA LaRC, http://www-air.larc.nasa.gov/data.htm), the National Center for Atmospheric Research Earth Observing Laboratory (NCAR EOL, http://data.eol.ucar.edu/), and the British Atmospheric Data Centre (BADC, http://badc.nerc.ac.uk). The geographical coverage is mainly the Pacific Ocean, with a few additional flights over the North Atlantic and the Indian Ocean, and near the North Pole (Fig. 9). Further details of the measurement campaigns are given in Table A1 in the Appendix. For the evaluation here, each measured concentration is assigned to a model grid point according to its location. Arithmetic averages are then computed for all samples available in the same latitude band (see Fig. 10) and longitude interval (1.875° on the T63 Gaussian grid) to produce the panels in the rightmost column of Fig. 10. As for model simulations, we first vertically interpolate the daily output to height levels, pick out the CN concentration occuring at the same location and in the same month as a measurement, then compute the sample average for each longitude and latitude band. The CN concentration in the model is

calculated by integrating the simulated number size distribution above the lower cut-off dry diameter (0.01 μm).

Figure 10 reveals that both model versions can correctly capture the main features of CN distribution at different locations. In the low latitude regions (Fig. 10a–f) the concentrations are highest in the upper troposphere [>4000 cm^{-3} STP (1013.25 hPa, 273.15 K)] due to strong nucleation, and decrease quickly towards the surface. In the Northern Hemisphere midlatitudes (Fig. 10g–i) the maxima at 120° E–180° and 100–60° W are caused by strong SO_2 sources in Asia and the USA. The air over Canada, Greenland and the Northern Polar Region is much cleaner (Figs. 9 and 10j–l).

Comparing the two HAM versions, we see that the new model produces in general better results. For example the high concentrations in the upper tropical troposphere in HAM2 (Fig. 10b, e) are closer to the observation. The east-west gradient in the upper troposphere over the Northwest Pacific (Fig. 10h) is better represented. The overestimation of CN concentrations in the clean regions is also reduced in HAM2 (Fig. 10, last row). Note that the observations suggest very high CN concentrations (>4000 cm^{-3} STP) in the surface layers over the SO_2 source regions (Fig. 10i). This feature is missing in the standard HAM1 and HAM2 simulations, but can be reproduced in HAM2 with the kinetic nucleation scheme of Kuang et al. (2008). Inclusion of the cluster activation scheme (Kulmala et al., 2006; Riipinen et al., 2007; Kazil et al., 2010) can also improve the results, but not as satisfactorily. The results are shown in Fig. 11.

5.3 Aerosol size distribution in the boundary layer

In observational studies it is a common practice to fit the measured aerosol number concentrations into log-normal probability density functions and summarize their characteristics by a few parameters. Such records are relatively straightforward to use in our model evaluation since HAM uses the same modal method to describe aerosol size distribution.

In Figs. 12 and 13 the three-mode distribution functions derived by Putaud et al. (2003) and Tunved et al. (2003) from measurements at six European surface sites (Harwell, Hohenpeissenberg, Aspvretren and Ispra from 1997 to 2001, Pallas and Hyytiälä in 2000 and 2001) are compared with HAM simulations in different seasons. In addition to the standard HAM1 and HAM2 simulations, the two sensitivity experiments discussed in the previous subsection (cf. Fig. 11) are also shown. On the whole the model does a very good job in reproducing the correct magnitude of aerosol number concentration at these locations. In winter, all HAM2 simulations are very similar. Compared to HAM1 there is a slight shift of the distribution functions towards larger sizes, possibly related to enhanced particle growth due to changes in the surface condensation of H_2SO_4 gas (cf. Fig. 2, bottom row). In summer, stronger solar radiation enhances the oxidation of SO_2, resulting in high concentrations of sulfuric acid gas in the near surface layers. Under such conditions, the model results become sensitive to the nucleation scheme. Consistent with Fig. 11, Fig. 13 reveals a clear increase in the number concentration of small particles when kinetic nucleation is included (solid green lines in the figure), and a moderate increase when the cluster activation scheme is used (dotted green lines). Figure 11 and Fig. 10i indicate a significant underestimate of particle concentration in heavily polluted areas even when additional nucleation mechanisms are included. In the cleaner regions (Fig. 13), however, such modifications lead to positive biases. This seems to suggest that the regional gradient in aerosol concentrations is underestimated. The reason might be inaccuracies in the emission of aerosols and their precursors, and/or the model representation of aerosol microphysics processes or meteorological conditions. So far we have not yet been able to collect sufficiently detailed, consistent and accurate observational data to help pinpoint the cause of these biases. Further studies are needed to address this issue.

For the marine boundary layer there exists a 30-yr climatology compiled by Heintzenberg et al. (2000) with relatively large geographical coverage. Using measurements obtained in a number of $15° \times 15°$ (latitude $\times$ logitude) regions (Fig. 14k), they derived the number concentration, geometric mean diameter and standard deviation of the Aitken

and accumulation modes for 10 latitude bands (see Table 3 therein). In Fig. 14 we compare this data set (black curves) with the standard HAM1 and HAM2 simulations (red and blue curves). In contrast to continental areas, the remote oceans are characterized by well-defined and clearly separated Aitken and accumulation mode. This feature is correctly captured in both model versions. In HAM1 the number concentration of the Aitken mode is considerably higher than accumulation mode in all latitude bands. The contrast is less pronounced in HAM2 because the modified sea salt emission scheme increases the emission flux of the accumulation mode (cf. Sect. 4.4), bringing the HAM2 results closer to observation, especially in the middle and low latitudes. The simulated distribution functions are generally broader than the Heintzenberg et al. (2000) dataset, due to the fact that the prescribed standard deviation (1.59 for both modes) is often larger than observed (typically 1.4–1.5).

5.4 Radiative properties of aerosols

The ultimate goal of simulating aerosols in a climate model is to understand their impact on climate. In this subsection we look at the simulated aerosol radiative properties that determine the direct and semi-direct aerosol effects in our model.

The top row of Fig. 15 presents the geographical distribution of annual mean AOD and Ångström parameter (ANG) from the MODIS data. The largest AOD appears in the polluted areas and in regions of high dust loading, while medium values are seen over the storm tracks. The retrieved Ångström parameters indicate that fine particles dominate the aerosol population over the continents and in the polar regions, while coarse particles are abundant over the storm tracks and in the tropical Atlantic. The HAM2 model reasonably reproduces these features of the global AOD and ANG distributions (Fig. 15, second row).

The differences between HAM2 and HAM1 shown in the middle and bottom rows of Fig. 15 are the combined effects of modified aerosol nucleation and water uptake parameterization, cloud microphysics, as well as the treatment of SOA. In the dust-dominated regions there is a marked increase in AOD and decrease in the Ångström

Aerosol properties in ECHAM-HAM2

K. Zhang et al.

Back | Close

Full Screen / Esc

Printer-friendly Version

Interactive Discussion

parameter (suggesting increase in particle size). Over the middle- and low-latitude ocean surfaces the AOD and particle size both become smaller, reflecting the decreased aerosol water amount as a consequence of the new water uptake scheme (Sect. 4.3). In the Southern Hemisphere storm track there are only small changes in AOD but substantial increases in the Ångström parameter (Fig. 15f), resulting from the shift of size distribution of the sea salt emission and reduced aerosol water uptake. Near the region 60–140° E, 50–60° S there are singularities in the relative differences of the Ångström parameter where large positive values change abruptly into large negative values. This is because HAM1 simulated a large amount of coarse mode particles in this area which gave negative Ångström parameters of small absolute value.

These changes have brought the model results closer to the MODIS data, although there is still room for improvement. In Western China and the Middle East and over the Arabian Peninsula, where dust is the dominant aerosol type, the model still has positive biases in ANG and negative biases in AOD, suggesting the dust emissions are not yet strong enough. The overestimation of AOD in Eastern US and Central Europe, as well as underestimation over the high-latitude continental areas, needs to be addressed in the future. A further increase of ANG over the storm tracks is also desirable.

The magnitude and distribution of aerosol absorption optical depth (AAOD) are key for atmospheric absorption, direct aerosol and the semi-direct aerosol radiative effects. Fig. 16 shows the simulated annual mean global distribution (panels a–c) together with the reference result compiled by Kinne (2009) (panel d) using the multi-model median from the AeroCom project and measurements from the NASA AERONET program (http://aeronet.gsfc.nasa.gov). The main contributors are black carbon and dust, rendering high values over the middle- and low-latitude continents. The characteristic spatial pattern is well represented by both HAM versions, but with a significant systematic underestimation of AAOD in HAM1 over the whole globe. The negative bias has been reduced in HAM2, partly because the refractive index of black carbon (BC) has been changed according to the medium-absorbing values from Bond and Bergstrom (2006), which improves the simulated AAOD near the source regions (but not in remote

areas, e.g. the Arctic regions). The other reason for this improvement is the weaker wet scavenging that increases the lifetime of BC, and consequently the overall BC burden.

To have a closer look at the model results beyond annual mean, and compare them with observation, we use the daily mean data of the year 2000 from AERONET. A map of the site locations is presented in Fig. 17. Daily mean model output is interpolated to the sites and sampled on the same days to derive the probability density functions (PDFs) shown in Fig. 18. For AOD the joint PDF of HAM2 vs HAM1 (Fig. 18c) features an elongated shape located near the diagonal of the diagram, indicating that results from the two versions are by and large similar. On the other hand, there is a clear increase of AOD in HAM2 in the clean regions as indicated by the upward bending of the "cloud" near the bottom left corner of the diagram in Fig. 18c. Although AERONET rarely observed AOD below 2×10^{-2}, HAM1 tends to produce very small values (Fig. 18a) in the high latitudes. Such underestimates have been reduced in HAM2, making the joint PDF in Fig. 18b better centered along the diagonal. As for the Ångström parameter, the modified sea salt emission has reduced the number of cases of too large particles (small values of the Ångström parameter, Fig. 18d–e), while there is still a substantial number of cases of overestimated Ångström parameter that need to be improved in the future. Figure 17 provides a summary of the model performance at each of the AERONET site.

5.5 Aerosol radiative forcing

The global mean values of AOD and AAOD in HAM1 and HAM2 are illustrated in Fig. 19. The AOD is further decomposed into contributions from aerosol water and dry mass. (In our model this diagnostic calculation is performed using the volume fractions of individual components and AOD of each mode.) The dry and water AOD are diagnosed as volume-weighted attribution of AOD. In both versions, water makes up more than two thirds of the total AOD. From HAM1 to the standard version of HAM2 there is a moderate increase in the dry AOD which is overcompensated by the decrease in aerosol water. The absorption AOD is increased by a factor of 2 from HAM1

to standard HAM2. For HAM2 the whiskers in the figure indicate the spread in the sensitivity experiments discussed in Sect. 4, giving a sense of uncertainties in this quantity. The lowest values (of total, water and dry AOD) are all associated with the Lohmann and Roeckner (1996) cloud microphysics parameterization, while the highest values of the total and water AOD are from the simulation using the old water uptake scheme (Table A2).

For all the HAM2 simulations we have diagnosed the various components of aerosol radiative forcing and illustrated the results in Fig. 20. On the global scale the scattering of shortwave radiation (cooling) overwhelms the absorption of longwave radiation (warming), rendering a total direct forcing of $-1.76\,\mathrm{W\,m^{-2}}$ at the top of the atmosphere (TOA) in standard HAM2. The various parameterization schemes discussed in this study exhibit considerable variation in the forcing, as can be seen from the whiskers. The numbers behind the bar chart are given in the Appendix (Table A2). Again we see a strong sensitivity of the model result to the water uptake scheme (experiment HAM2_WAT) and cloud microphysics (autoconversion, experiment HAM2_CLD), both at TOA and at the Earth's surface.

6 Conclusions

This study introduces improved aerosol representations in the second version of the ECHAM-HAM model and quantifies their impact on the simulated aerosol properties, global distribution, and direct radiative effects. Some of the model improvments, for example in the sea salt and dust emissions, were directly motivated by previously noticed model biases. The others aimed at having a more physically realistic representation of the aerosol lifecycle and extending the model's capability in consistently simulating the interactions between various aerosol-related micro- and macro-scale processes. The new H_2SO_4/H_2O aerosol nucleation scheme considers both neutral and charged nucleation, which can be used to investigate the impact of nucleation from ions caused by cosmic rays (Kazil et al., 2010) and by radioactive species effusing from the Earth's

surface (Zhang et al., 2011). The explicit treatment of SOA introduced by O'Donnell et al. (2011) can be used to investigate, for instance, the impact of vegetation change on aerosol formation and the consequent changes in cloud radiative forcing. The coupling to a two-moment stratiform cloud microphysics scheme (Lohmann et al., 2007) makes it possible for this model to directly simulate the aerosol indirect effects on climate.

The impacts of these updates on the simulated aerosol distributions and properties are analyzed in Sects. 4 and 5. The new parameterizations that have largest impact on the global mean AOD and aerosol radiative effects are the water uptake scheme and the new stratiform cloud microphysics. The water uptake scheme implemented by O'Donnell et al. (2011) considerably reduces the aerosol water content in the lower troposphere. The (global) total mass of aerosol water is in closer agreement with the AeroCom multi-model mean. The new stratiform cloud microphysics features weaker autoconversion compared to the scheme of Lohmann and Roeckner (1996) Lohmann and Roeckner (1996), which contributes to changes to aerosol lifetime and wet deposition. Compared to HAM1, aerosol lifetimes are increased in HAM2 for all aerosol species except for sea salt (by 10–20 % for sulfate, black carbon, and POA, 107 % for SOA, and 4 % for dust). Wet deposition is decreased for all aerosol species except for particulate organic matter.

The modified sea salt emission calculation significantly changes the partitioning of particle number fluxes between accumulation mode and coarse mode, resulting in a shift of the size distribution to smaller particles. The nucleation parameterization of Kazil et al. (2010) leads to an upward shift of the strongest nucleation to the tropical tropopause. Although the resulting changes in the spatial distribution of nucleation mode number concentration are nontrivial, the changes in the direct aerosol effect are relatively small because of the small sizes of the particles.

By including all these updates in the model, we are able to obtain improved results compared to HAM1. As shown in Sects. 5.2–5.4, the aerosol size distribution and spatial-temporal variability simulated by HAM2 show better agreement with the

Aerosol properties in ECHAM-HAM2

K. Zhang et al.

observations. The simulated AAOD in HAM2 agrees better with the reference result. The remaining major model deficiencies include (i) positive bias of AOD over the storm tracks, (ii) negative bias of AOD and aerosol mass concentration in high-latitude regions, and (iii) negative bias of particle number concentration, especially that of the Aitken mode, in the lower troposphere over the heavily polluted regions.

There are a few other modifications that have already been implemented in the model but not switched on in the standard HAM2. Aerosol formation by cluster activation (Kulmala et al., 2006; Riipinen et al., 2007) or by kinetic nucleation (Laakso et al., 2004; Kuang et al., 2008) improve near-surface aerosol number concentrations in the polluted regions, but would lead to overestimation in cleaner continental regions. The inclusion of the temperature-dependent in-cloud scavenging scheme for mixed-phase clouds and the below-cloud scavenging scheme of Croft et al. (2009) that takes into account of aerosol and collector sizes seem to have some positive impact on model results, but more extensive evaluation is still needed.

In this study the evaluation was concentrated mainly on the global distribution and the radiative properties of aerosols. With the new two-moment cloud microphysics implemented, it is possible to investigate the aerosol effect on cloud via the first indirect effect and/or the second indirect effect. It is worthwhile studying the indirect effects of anthropogenic aerosols on climate in our model and their sensitivity to model configuration and resolution, not only in nudged integrations, but in "free" climate simulations. These will be presented in separate papers. Furthermore, the aerosol activation scheme used in this model version is still rather simple and empirical. A more physically-based scheme has been implemented and evaluation (Stier et al., 2012). A new scheme for the in-cloud aerosol scavenging has been developed recently by Croft et al. (2010), which may help achieve a treatment that is consistent with the cloud microphysics in the model and reduce biases.

References

Abdul-Razzak, H. and Ghan, S. J.: A parameterization of aerosol activation - 2. multiple aerosol types, J. Geophys. Res., 105, 6837–6844, doi:10.1029/1999JD901161, 2000. 7563

Bauer, S. E., Wright, D. L., Koch, D., Lewis, E. R., McGraw, R., Chang, L.-S., Schwartz, S. E., and Ruedy, R.: MATRIX (Multiconfiguration Aerosol TRacker of mIXing state): an aerosol microphysical module for global atmospheric models, Atmos. Chem. Phys., 8, 6003–6035, doi:10.5194/acp-8-6003-2008, 2008. 7547

Bergman, T., Kerminen, V.-M., Korhonen, H., Lehtinen, K. J., Makkonen, R., Arola, A., Mielonen, T., Romakkaniemi, S., Kulmala, M., and Kokkola, H.: Evaluation of the sectional aerosol microphysics module SALSA implementation in ECHAM5-HAM aerosol-climate model, Geosci. Model Dev. Discuss., 4, 3623–3690, doi:10.5194/gmdd-4-3623-2011, 2011. 7548

Bond, T. C. and Bergstrom, R. W.: Light Absorption by Carbonaceous Particles: An Investigative Review, Aerosol Sci. Technol., 40, 27–67, doi:10.1080/02786820500421521, 2006. 7569

Bourgeois, Q. and Bey, I.: Pollution transport efficiency toward the Arctic: Sensitivity to aerosol scavenging and source regions, J. Geophys. Res., 116, D08213, doi:10.1029/2010JD015096, 2011. 7548

Cagnazzo, C., Manzini, E., Giorgetta, M. A., Forster, P. M. De F., and Morcrette, J. J.: Impact of an improved shortwave radiation scheme in the MAECHAM5 General Circulation Model, Atmos. Chem. Phys., 7, 2503–2515, doi:10.5194/acp-7-2503-2007, 2007. 7549, 7585

Discussion Paper | Discussion Paper | Discussion Paper | Discussion Paper |

ACPD

12, 7545–7615, 2012

Aerosol properties in ECHAM-HAM2

K. Zhang et al.

Title Page

Abstract | Introduction

Conclusions | References

Tables | Figures

◀ | ▶

◀ | ▶

Back | Close

Full Screen / Esc

Printer-friendly Version

Interactive Discussion

Cheng, T., Peng, Y., Feichter, J., and Tegen, I.: An improvement on the dust emission scheme in the global aerosol-climate model ECHAM5-HAM, Atmos. Chem. Phys., 8, 1105–1117, doi:10.5194/acp-8-1105-2008, 2008. 7549, 7559, 7585

Croft, B., Lohmann, U., Martin, R. V., Stier, P., Wurzler, S., Feichter, J., Posselt, R., and Ferrachat, S.: Aerosol size-dependent below-cloud scavenging by rain and snow in the ECHAM5-HAM, Atmos. Chem. Phys., 9, 4653–4675, doi:10.5194/acp-9-4653-2009, 2009. 7548, 7549, 7561, 7573, 7585, 7586, 7599

Croft, B., Lohmann, U., Martin, R. V., Stier, P., Wurzler, S., Feichter, J., Hoose, C., Heikkilä, U., van Donkelaar, A., and Ferrachat, S.: Influences of in-cloud aerosol scavenging parameterizations on aerosol concentrations and wet deposition in ECHAM5-HAM, Atmos. Chem. Phys., 10, 1511–1543, doi:10.5194/acp-10-1511-2010, 2010. 7573

Dentener, F., Kinne, S., Bond, T., Boucher, O., Cofala, J., Generoso, S., Ginoux, P., Gong, S., Hoelzemann, J. J., Ito, A., Marelli, L., Penner, J. E., Putaud, J.-P., Textor, C., Schulz, M., van der Werf, G. R., and Wilson, J.: Emissions of primary aerosol and precursor gases in the years 2000 and 1750 prescribed data-sets for AeroCom, Atmos. Chem. Phys., 6, 4321–4344, doi:10.5194/acp-6-4321-2006, 2006. 7552, 7555, 7556, 7559, 7564, 7585

Easter, R. C., Ghan, S. J., Zhang, Y., Saylor, R. D., Chapman, E. G., Laulainen, N. S., Abdul-Razzak, H., Leung, L. R., Bian, X., and Zaveri, R. A.: MIRAGE: Model description and evaluation of aerosols and trace gases, J. Geophys. Res., 109, D20210, doi:10.1029/2004JD004571, 2004. 7547

Feichter, J., Kjellström, E., Rodhe, H., Dentener, F., Lelieveld, J., and Roelofs, G. J.: Simulation of the tropospheric sulfur cycle in a global climate model., Atmos. Environ., 30, 1693–1707, doi:10.1016/1352-2310(95)00394-0, 1996. 7547, 7551

Fischer-Bruns, I., Feichter, J., Kloster, S., and Schneidereit, A.: How present aerosol pollution from North America impacts North Atlantic climate, Tellus A, 62, 579–589, doi:10.1111/j.1600-0870.2010.00446.x, 2010. 7548

Folini, D. and Wild, M.: Aerosol emissions and dimming/brightening in Europe: Sensitivity studies with ECHAM5-HAM, J. Geophys. Res., 116, D21104, doi:10.1029/2011JD016227, 2011. 7548

Fouquart, Y. and Bonnel, B.: Computations of solar heating of the earth's atmosphere: A new parameterization., Beitr. Phys. Atmos., 53, 35–62, 1980. 7585

Title Page

Abstract | Introduction

Conclusions | References

Tables | Figures

◄◄ | ►►

◄ | ►

Back | Close

Full Screen / Esc

Printer-friendly Version

Interactive Discussion

Guelle, W., Schulz, M., Balkanski, Y., and Dentener, F.: Influence of the source formulation on modeling the atmospheric global distribution of sea salt aerosol., J. Geophys. Res., 106, 27509–27524, 2001. 7550

Heintzenberg, J., Covert, D. C., and van Dingenen, R.: Size distribution and chemical composition of marine aerosols: a compilation and review, Tellus, 52B, 1104–1122, doi:10.1034/j.1600-0889.2000.00136.x, 2000. 7567, 7568, 7607

Hoose, C., Lohmann, U., Bennartz, R., Croft, B., and Lesins, G.: Global simulations of aerosol processing in clouds, Atmos. Chem. Phys., 8, 6939–6963, doi:10.5194/acp-8-6939-2008, 2008. 7548

Horowitz, L. W., Walters, S., Mauzerall, D. L., Emmons, L. K., Rasch, P. J., Granier, C., Tie, X., Lamarque, J.-F., Schultz, M. G., Tyndall, G. S., Orlando, J. J., and Brasseur, G. P.: A global simulation of tropospheric ozone and related tracers: Description and evaluation of MOZART, version 2., J. Geophys. Res., 108, 4784, doi:10.1029/2002JD002853, 2003. 7551

Jacobson, M. Z.: Global direct radiative forcing due to molticomponent anthropogenic and natural aerosols., J. Geophys. Res., 106, 1551–1568, doi:10.1029/2000JD900514, 2001. 7547

Kanakidou, M., Seinfeld, J. H., Pandis, S. N., Barnes, I., Dentener, F. J., Facchini, M. C., Van Dingenen, R., Ervens, B., Nenes, A., Nielsen, C. J., Swietlicki, E., Putaud, J. P., Balkanski, Y., Fuzzi, S., Horth, J., Moortgat, G. K., Winterhalter, R., Myhre, C. E. L., Tsigaridis, K., Vignati, E., Stephanou, E. G., and Wilson, J.: Organic aerosol and global climate modelling: a review, Atmos. Chem. Phys., 5, 1053–1123, doi:10.5194/acp-5-1053-2005, 2005. 7555

Kärcher, B. and Lohmann, U.: A parameterization of cirrus cloud formation: Heterogeneous freezing, J. Geophys. Res.-Atmos., 108, 4402, doi:10.1029/2002JD003220, 2003. 7562

Kazil, J. and Lovejoy, E. R.: A semi-analytical method for calculating rates of new sulfate aerosol formation from the gas phase, Atmos. Chem. Phys., 7, 3447–3459, doi:10.5194/acp-7-3447-2007, 2007. 7553, 7554

Kazil, J., Stier, P., Zhang, K., Quaas, J., Kinne, S., O'Donnell, D., Rast, S., Esch, M., Ferrachat, S., Lohmann, U., and Feichter, J.: Aerosol nucleation and its role for clouds and Earth's radiative forcing in the aerosol-climate model ECHAM5-HAM, Atmos. Chem. Phys., 10, 10733–10752, doi:10.5194/acp-10-10733-2010, 2010. 7549, 7553, 7554, 7566, 7571, 7572, 7585, 7587, 7595, 7604

Kazil, J., Zhang, K., Stier, P., Feichter, J., Lohmann, U., and O'Brien, K.: The present-day decadal solar cycle modulation of Earth's radiative forcing via charged H2SO4/H2O aerosol nucleation, Geophys. Res. Lett., 39, L02805, doi:10.1029/2011GL050058, 2012. 7548

Khairoutdinov, M. and Kogan, Y.: A New Cloud Physics Parameterization in a Large-Eddy Simulation Model of Marine Stratocumulus, Mon. Weather Rev., 128, 229, doi:10.1175/1520-0493(2000)128¡0229:ANCPPI¿2.0.CO;2, 2000. 7562

Kinne, S.: Climatologies of Cloud-related Aerosols: Part 1: Particle number and size, 37–57, The MIT Press, Cambridge, MA, 2009. 7569

Kinne, S., Schulz, M., Textor, C., Guibert, S., Balkanski, Y., Bauer, S. E., Berntsen, T., Berglen, T. F., Boucher, O., Chin, M., Collins, W., Dentener, F., Diehl, T., Easter, R., Feichter, J., Fillmore, D., Ghan, S., Ginoux, P., Gong, S., Grini, A., Hendricks, J., Herzog, M., Horowitz, L., Isaksen, I., Iversen, T., Kirkevåg, A., Kloster, S., Koch, D., Kristjansson, J. E., Krol, M., Lauer, A., Lamarque, J. F., Lesins, G., Liu, X., Lohmann, U., Montanaro, V., Myhre, G., Penner, J., Pitari, G., Reddy, S., Seland, O., Stier, P., Takemura, T., and Tie, X.: An AeroCom initial assessment – optical properties in aerosol component modules of global models, Atmos. Chem. Phys., 6, 1815–1834, doi:10.5194/acp-6-1815-2006, 2006. 7547

Kloster, S., Feichter, J., Maier-Reimer, E., Six, K. D., Stier, P., and Wetzel, P.: DMS cycle in the marine ocean-atmosphere system – a global model study, Biogeosciences, 3, 29–51, doi:10.5194/bg-3-29-2006, 2006. 7550

Kloster, S., Dentener, F., Feichter, J., Raes, F., van Aardenne, J., Roeckner, E., Lohmann, U., Stier, P., and Swart, R.: Influence of future air pollution mitigation strategies on total aerosol radiative forcing, Atmos. Chem. Phys., 8, 6405–6437, doi:10.5194/acp-8-6405-2008, 2008. 7548

Koch, D., Schulz, M., Kinne, S., McNaughton, C., Spackman, J. R., Balkanski, Y., Bauer, S., Berntsen, T., Bond, T. C., Boucher, O., Chin, M., Clarke, A., De Luca, N., Dentener, F., Diehl, T., Dubovik, O., Easter, R., Fahey, D. W., Feichter, J., Fillmore, D., Freitag, S., Ghan, S., Ginoux, P., Gong, S., Horowitz, L., Iversen, T., Kirkevåg, A., Klimont, Z., Kondo, Y., Krol, M., Liu, X., Miller, R., Montanaro, V., Moteki, N., Myhre, G., Penner, J. E., Perlwitz, J., Pitari, G., Reddy, S., Sahu, L., Sakamoto, H., Schuster, G., Schwarz, J. P., Seland, Ø., Stier, P., Takegawa, N., Takemura, T., Textor, C., van Aardenne, J. A., and Zhao, Y.: Evaluation of black carbon estimations in global aerosol models, Atmos. Chem. Phys., 9, 9001–9026, doi:10.5194/acp-9-9001-2009, 2009. 7548

Kokkola, H., Hommel, R., Kazil, J., Niemeier, U., Partanen, A.-I., Feichter, J., and Timmreck, C.: Aerosol microphysics modules in the framework of the ECHAM5 climate model – intercomparison under stratospheric conditions, Geosci. Model Dev., 2, 97–112, doi:10.5194/gmd-2-97-2009, 2009. 7554, 7555, 7585

Kuang, C., McMurry, P. H., McCormick, A. V., and Eisele, F. L.: Dependence of nucleation rates on sulfuric acid vapor concentration in diverse atmospheric locations, J. Geophys. Res., 113, D10209, doi:10.1029/2007JD009253, 2008. 7553, 7566, 7573, 7585, 7604

Kulmala, M., Laaksonen, A., and Pirjola, L.: Parameterizations for sulfuric acid/water nucleation rates, J. Geophys. Res., 103, 8301–8307, doi:10.1029/97JD03718, 1998. 7553, 7585, 7587

Kulmala, M., Lehtinen, K. E. J., and Laaksonen, A.: Cluster activation theory as an explanation of the linear dependence between formation rate of 3 nm particles and sulphuric acid concentration, Atmos. Chem. Phys., 6, 787–793, doi:10.5194/acp-6-787-2006, 2006. 7553, 7566, 7573, 7585, 7604

Kulmala, M., Asmi, A., Lappalainen, H. K., Baltensperger, U., Brenguier, J.-L., Facchini, M. C., Hansson, H.-C., Hov, ØØ., O'Dowd, C. D., Pöschl, U., Wiedensohler, A., Boers, R., Boucher, O., de Leeuw, G., Denier van der Gon, H. A. C., Feichter, J., Krejci, R., Laj, P., Lihavainen, H., Lohmann, U., McFiggans, G., Mentel, T., Pilinis, C., Riipinen, I., Schulz, M., Stohl, A., Swietlicki, E., Vignati, E., Alves, C., Amann, M., Ammann, M., Arabas, S., Artaxo, P., Baars, H., Beddows, D. C. S., Bergström, R., Beukes, J. P., Bilde, M., Burkhart, J. F., Canonaco, F., Clegg, S. L., Coe, H., Crumeyrolle, S., D'Anna, B., Decesari, S., Gilardoni, S., Fischer, M., Fjaeraa, A. M., Fountoukis, C., George, C., Gomes, L., Halloran, P., Hamburger, T., Harrison, R. M., Herrmann, H., Hoffmann, T., Hoose, C., Hu, M., Hyvärinen, A., Hõrrak, U., Iinuma, Y., Iversen, T., Josipovic, M., Kanakidou, M., Kiendler-Scharr, A., Kirkevåg, A., Kiss, G., Klimont, Z., Kolmonen, P., Komppula, M., Kristjánsson, J.-E., Laakso, L., Laaksonen, A., Labonnote, L., Lanz, V. A., Lehtinen, K. E. J., Rizzo, L. V., Makkonen, R., Manninen, H. E., McMeeking, G., Merikanto, J., Minikin, A., Mirme, S., Morgan, W. T., Nemitz, E., O'Donnell, D., Panwar, T. S., Pawlowska, H., Petzold, A., Pienaar, J. J., Pio, C., Plass-Duelmer, C., Prévôt, A. S. H., Pryor, S., Reddington, C. L., Roberts, G., Rosenfeld, D., Schwarz, J., Seland, Ø., Sellegri, K., Shen, X. J., Shiraiwa, M., Siebert, H., Sierau, B., Simpson, D., Sun, J. Y., Topping, D., Tunved, P., Vaattovaara, P., Vakkari, V., Veefkind, J. P., Visschedijk, A., Vuollekoski, H., Vuolo, R., Wehner, B., Wildt, J., Woodward, S., Worsnop, D. R., van Zadelhoff, G.-J., Zardini, A. A., Zhang, K., van Zyl, P. G., Kerminen, V.-M., S Carslaw, K., and Pandis, S. N.: General overview: European Integrated project on Aerosol Cloud Climate and Air Quality interactions (EUCAARI) – integrating aerosol research from nano to global scales, Atmos. Chem. Phys., 11, 13061–13143, doi:10.5194/acp-11-13061-2011, 2011. 7547

Laakso, L., Petäjä, T., Lehtinen, K. E. J., Kulmala, M., Paatero, J., Hõrrak, U., Tammet, H., and Joutsensaari, J.: Ion production rate in a boreal forest based on ion, particle and radiation

Title Page

Abstract | Introduction

Conclusions | References

Tables | Figures

◀ | ▶

◀ | ▶

Back | Close

Full Screen / Esc

Printer-friendly Version

Interactive Discussion

measurements, Atmos. Chem. Phys., 4, 1933–1943, doi:10.5194/acp-4-1933-2004, 2004. 7553, 7573

Langner, J. and Rodhe, H.: A global three-dimensional model of the tropospheric sulfur cycle, J. Atmos. Chem., 13, 225–263, doi:10.1007/BF00058134, 1991. 7547

5   Laurent, B., Marticorena, B., Bergametti, G., and Mei, F.: Modeling mineral dust emissions from Chinese and Mongolian deserts, Global Planet. Change, 52, 121–141, doi:10.1016/j.gloplacha.2006.02.012, 2006. 7559

Lin, H. and Leaitch, W. R.: Development of an in-cloud aerosol activation parameterization for climate modelling., in: WMO Workshop on Measurement of Cloud Properties for Forecasts
10   of Weather, Air Quality and Climate, 328–355, Geneva, Switzerland, World Meteorology Organization, 1997. 7562, 7563

Liu, X., Penner, J. E., and Herzog, M.: Global modeling of aerosol dynamics: Model description, evaluation, and interactions between sulfate and nonsulfate aerosols, J. Geophys. Res., 110, D18206, doi:10.1029/2004JD005674, 2005. 7547

15   Liu, X., Easter, R. C., Ghan, S. J., Zaveri, R., Rasch, P., Shi, X., Lamarque, J.-F., Gettelman, A., Morrison, H., Vitt, F., Conley, A., Park, S., Neale, R., Hannay, C., Ekman, A. M. L., Hess, P., Mahowald, N., Collins, W., Iacono, M. J., Bretherton, C. S., Flanner, M. G., and Mitchell, D.: Toward a minimal representation of aerosol direct and indirect effects: model description and evaluation, Geosci. Model Dev. Discuss., 4, 3485–3598, doi:10.5194/gmdd-4-3485-
20   2011, 2011. 7547

Lohmann, U. and Ferrachat, S.: Impact of parametric uncertainties on the present-day climate and on the anthropogenic aerosol effect, Atmos. Chem. Phys., 10, 11373–11383, doi:10.5194/acp-10-11373-2010, 2010. 7563

Lohmann, U. and Hoose, C.: Sensitivity studies of different aerosol indirect effects in mixed-
25   phase clouds, Atmos. Chem. Phys., 9, 8917–8934, doi:10.5194/acp-9-8917-2009, 2009. 7548, 7562

Lohmann, U. and Roeckner, E.: Design and performance of a new cloud microphysics scheme developed for the ECHAM general circulation model, Clim. Dynam., 12, 557–572, doi:10.1007/BF00207939, 1996. 7561, 7562, 7563, 7571, 7572, 7585, 7586, 7591, 7600

30   Lohmann, U., Stier, P., Hoose, C., Ferrachat, S., Kloster, S., Roeckner, E., and Zhang, J.: Cloud microphysics and aerosol indirect effects in the global climate model ECHAM5-HAM, Atmos. Chem. Phys., 7, 3425–3446, doi:10.5194/acp-7-3425-2007, 2007. 7549, 7562, 7572, 7585, 7591

Aerosol properties in ECHAM-HAM2

K. Zhang et al.

Title Page

Abstract   Introduction

Conclusions   References

Tables   Figures

◄◄   ►►

◄   ►

Back   Close

Full Screen / Esc

Printer-friendly Version

Interactive Discussion

Makkonen, R., Asmi, A., Korhonen, H., Kokkola, H., Järvenoja, S., Räisänen, P., Lehtinen, K. E. J., Laaksonen, A., Kerminen, V.-M., Järvinen, H., Lohmann, U., Bennartz, R., Feichter, J., and Kulmala, M.: Sensitivity of aerosol concentrations and cloud properties to nucleation and secondary organic distribution in ECHAM5-HAM global circulation model, Atmos. Chem. Phys., 9, 1747–1766, doi:10.5194/acp-9-1747-2009, 2009. 7548

Mashayekhi, R., Irannejad, P., Feichter, J., and Bidokhti, A. A.: Implementation of a new aerosol HAM model within the Weather Research and Forecasting (WRF) modeling system, Geosci. Model Dev. Discuss., 2, 681–707, doi:10.5194/gmdd-2-681-2009, 2009. 7548

Monahan, E., Spiel, D., and Davidson, K.: A model of marine aerosol generation via whitecaps and wave disruption, in: Oceanic whitecaps and their role in air-sea exchange, Reidel, D., 167–174, Norwell, Massachusetts, 1986. 7558, 7585, 7597

Ng, N. L., Chhabra, P. S., Chan, A. W. H., Surratt, J. D., Kroll, J. H., Kwan, A. J., McCabe, D. C., Wennberg, P. O., Sorooshian, A., Murphy, S. M., Dalleska, N. F., Flagan, R. C., and Seinfeld, J. H.: Effect of NO_x level on secondary organic aerosol (SOA) formation from the photooxidation of terpenes, Atmos. Chem. Phys., 7, 5159–5174, doi:10.5194/acp-7-5159-2007, 2007. 7556

Niemeier, U., Timmreck, C., Graf, H.-F., Kinne, S., Rast, S., and Self, S.: Initial fate of fine ash and sulfur from large volcanic eruptions, Atmos. Chem. Phys., 9, 9043–9057, doi:10.5194/acp-9-9043-2009, 2009. 7548, 7550

Niemeier, U., Schmidt, H., and Timmreck, C.: The dependency of geoengineered sulfate aerosol on the emission strategy, Atmos. Sci. Lett., 12, 189–194, doi:10.1002/asl.304, 2011. 7548

O'Donnell, D., Tsigaridis, K., and Feichter, J.: Estimating the direct and indirect effects of secondary organic aerosols using ECHAM5-HAM, Atmos. Chem. Phys., 11, 8635–8659, doi:10.5194/acp-11-8635-2011, 2011. 7549, 7555, 7556, 7557, 7572, 7585, 7596

Odum, J. R., T. Hoffman, T., Bowman, F., Collins, D., Flagan, R. C., and Seinfeld, J. H.: Gas/Particle Partitioning and Secondary Organic Aerosol Yields, Environ. Sci. Technol., 30, 2580–2585, doi:10.1021/es950943+, 1996. 7556

Petters, M. D. and Kreidenweis, S. M.: A single parameter representation of hygroscopic growth and cloud condensation nucleus activity, Atmos. Chem. Phys., 7, 1961–1971, doi:10.5194/acp-7-1961-2007, 2007. 7557, 7558, 7585, 7588

Pham, M., Müller, J. F., Brasseur, G. P., Granier, C., and Mégie, G.: A three-dimensional study of the tropospheric sulfur cycle, J. Geophys. Res., 100, 26061–26092, doi:10.1029/95JD02095, 1995. 7550

Prigent, C., Tegen, I., Aires, F., Marticorena, B., and Zribi, M.: Estimation of the aerodynamic roughness length in arid and semiarid regions over the globe with the ERS scatterometer, J. Geophys. Res., 110, D09205, doi:10.1029/2004JD005370, 2005. 7559

Pringle, K. J., Tost, H., Metzger, S., Steil, B., Giannadaki, D., Nenes, A., Fountoukis, C., Stier, P., Vignati, E., and Lelieveld, J.: Description and evaluation of GMXe: a new aerosol submodel for global simulations (v1), Geosci. Model Dev. Discuss., 3, 569–626, doi:10.5194/gmdd-3-569-2010, 2010. 7548

Putaud, J., van Dingenen, R., Baltensperger, U., Bruggemann, E., Charron, A., Facchini, M., Decesari, S., Fuzzi, S., Gehrig, R., H. H.-C., Harrison, R. M., Jones, A. M., Laj, P., Lorbeer, G., Maen- haut, W., Mihalopoulos, N., Müller, K., Palmgren, F., Querol, X., Rodriguez, S., Schneider, J., Spindler, G., ten Brink, H., Tunved, P., Torseth, K., Wehner, B., Weingartner, E., Wiedensohler, A., Wahlin, P., and Raes, F.: A European aerosol phenomenology; physical and chemical characteristics of particulate matter at kerbside, urban, rural and background sites in Europe, Tech. Rep. Report nr. EUR 20411, European Commission, 2003. 7567, 7605

Quaas, J., Boucher, O., and Breon, F. M.: Aerosol indirect effects in POLDER satellite data and the Laboratoire de Meteorologie Dynamique-Zoom (LMDZ) general circulation model, J. Geophys. Res., 109, D08205, doi:10.1029/2003JD004317, 2004. 7549

Riipinen, I., Sihto, S.-L., Kulmala, M., Arnold, F., Dal Maso, M., Birmili, W., Saarnio, K., Teinilä, K., Kerminen, V.-M., Laaksonen, A., and Lehtinen, K. E. J.: Connections between atmospheric sulphuric acid and new particle formation during QUEST III–IV campaigns in Heidelberg and Hyytiälä, Atmos. Chem. Phys., 7, 1899–1914, doi:10.5194/acp-7-1899-2007, 2007. 7553, 7566, 7573, 7585, 7604

Roeckner, E., Bäuml, G., Bonaventura, L., Brokopf, R., Esch, M., Giorgetta, M., Hagemann, S., Kirchner, I., Kornblueh, L., Manzini, E., Rhodin, A., Schlese, U., Schulzweida, U., and Tompkins, A.: The atmospheric general circulation model ECHAM 5. PART I: model description, MPI Technical Report 349, Max Planck Institute for Meteorology, Hamburg, Germany, 2003. 7548, 7550, 7585

Roeckner, E., Brokopf, R., Esch, M., Giorgetta, M. A., Hagemann, S., Kornblueh, L., Manzini, E., Schlese, U., and Schulzweida, U.: Sensitivity of Simulated Climate to Horizontal

and Vertical Resolution in the ECHAM5 Atmosphere Model, J. Climate, 19, 3771–3791, doi:10.1175/JCLI3824.1, 2006a. 7548, 7550, 7585

Roeckner, E., Stier, P., Feichter, J., Kloster, S., Esch, M., and Fischer-Bruns, I.: Impact of carbonaceous aerosol emissions on regional climate change, Clim. Dynam., 27, 553–571, doi:10.1007/s00382-006-0147-3, 2006b. 7548

Schulz, M., Textor, C., Kinne, S., Balkanski, Y., Bauer, S., Berntsen, T., Berglen, T., Boucher, O., Dentener, F., Guibert, S., Isaksen, I. S. A., Iversen, T., Koch, D., Kirkevåg, A., Liu, X., Montanaro, V., Myhre, G., Penner, J. E., Pitari, G., Reddy, S., Seland, Ø., Stier, P., and Takemura, T.: Radiative forcing by aerosols as derived from the AeroCom present-day and pre-industrial simulations, Atmos. Chem. Phys., 6, 5225–5246, doi:10.5194/acp-6-5225-2006, 2006. 7547

Schulz, M., Chin, M., and Kinne, S.: The Aerosol Model Comparison Project, AeroCom, Phase II: Clearing Up Diversity, IGAC Newsletter, 2009. 7549

Smith, M. and Harrison, N.: The sea spray generation function., J. Aerosol Sci., 29, 189–190, doi:10.1016/S0021-8502(98)00280-8, 1998. 7558, 7585, 7597

Spracklen, D. V., Pringle, K. J., Carslaw, K. S., Chipperfield, M. P., and Mann, G. W.: A global off-line model of size-resolved aerosol microphysics: I. Model development and prediction of aerosol properties, Atmos. Chem. Phys., 5, 2227–2252, doi:10.5194/acp-5-2227-2005, 2005. 7547

Stier, P., Feichter, J., Kinne, S., Kloster, S., Vignati, E., Wilson, J., Ganzeveld, L., Tegen, I., Werner, M., Balkanski, Y., Schulz, M., Boucher, O., Minikin, A., and Petzold, A.: The aerosol-climate model ECHAM5-HAM, Atmos. Chem. Phys., 5, 1125–1156, doi:10.5194/acp-5-1125-2005, 2005. 7547, 7548, 7550, 7551, 7555, 7558, 7560, 7561, 7565, 7585, 7586, 7594, 7596, 7615

Stier, P., Feichter, J., Roeckner, E., Kloster, S., and Esch, M.: The evolution of the global aerosol system in a transient climate simulation from 1860 to 2100, Atmos. Chem. Phys., 6, 3059–3076, doi:10.5194/acp-6-3059-2006, 2006. 7548

Stier, P., Seinfeld, J. H., Kinne, S., and Boucher, O.: Aerosol absorption and radiative forcing, Atmos. Chem. Phys., 7, 5237–5261, doi:10.5194/acp-7-5237-2007, 2007. 7548

Stokes, R. H. and Robinson, R. A.: Interactions in aqueous nonelectrolyte solutions. I. Solute-solvent equilibria, J. Phys. Chem., 70, 2126–2130, doi:10.1021/j100879a010, 1966. 7557, 7585

Title Page

Abstract | Introduction

Conclusions | References

Tables | Figures

|◀ | ▶|

◀ | ▶

Back | Close

Full Screen / Esc

Printer-friendly Version

Interactive Discussion

Tegen, I., Harrison, S. P., Kohfeld, K., Prentice, I. C., Coe, M., and Heimann, M.: Impact of vegetation and preferential source areas on global dust aerosol: Results from a model study, J. Geophys. Res., 107, 4576, doi:10.1029/2001JD000963, 2002. 7550, 7559, 7585

Textor, C., Schulz, M., Guibert, S., Kinne, S., Balkanski, Y., Bauer, S., Berntsen, T., Berglen, T., Boucher, O., Chin, M., Dentener, F., Diehl, T., Easter, R., Feichter, H., Fillmore, D., Ghan, S., Ginoux, P., Gong, S., Grini, A., Hendricks, J., Horowitz, L., Huang, P., Isaksen, I., Iversen, I., Kloster, S., Koch, D., Kirkevåg, A., Kristjansson, J. E., Krol, M., Lauer, A., Lamarque, J. F., Liu, X., Montanaro, V., Myhre, G., Penner, J., Pitari, G., Reddy, S., Seland, Ø., Stier, P., Takemura, T., and Tie, X.: Analysis and quantification of the diversities of aerosol life cycles within AeroCom, Atmos. Chem. Phys., 6, 1777–1813, doi:10.5194/acp-6-1777-2006, 2006. 7547, 7558, 7589, 7590

Textor, C., Schulz, M., Guibert, S., Kinne, S., Balkanski, Y., Bauer, S., Berntsen, T., Berglen, T., Boucher, O., Chin, M., Dentener, F., Diehl, T., Feichter, J., Fillmore, D., Ginoux, P., Gong, S., Grini, A., Hendricks, J., Horowitz, L., Huang, P., Isaksen, I. S. A., Iversen, T., Kloster, S., Koch, D., Kirkevåg, A., Kristjansson, J. E., Krol, M., Lauer, A., Lamarque, J. F., Liu, X., Montanaro, V., Myhre, G., Penner, J. E., Pitari, G., Reddy, M. S., Seland, Ø., Stier, P., Takemura, T., and Tie, X.: The effect of harmonized emissions on aerosol properties in global models – an AeroCom experiment, Atmos. Chem. Phys., 7, 4489–4501, doi:10.5194/acp-7-4489-2007, 2007. 7547

Timmreck, C., Graf, H. F., Lorenz, S. J., Niemeier, U., Zanchettin, D., Matei, D., Jungclaus, J. H., and Crowley, T. J.: Aerosol size confines climate response to volcanic super-eruptions, Geophys. Res. Lett., 37, L24705, doi:10.1029/2010GL045464, 2010. 7548

Tunved, P., Hansson, H.-C., Kulmala, M., Aalto, P., Viisanen, Y., Karlsson, H., Kristensson, A., Swietlicki, E., Dal Maso, M., Ström, J., and Komppula, M.: One year boundary layer aerosol size distribution data from five nordic background stations, Atmos. Chem. Phys., 3, 2183–2205, doi:10.5194/acp-3-2183-2003, 2003. 7567, 7605

Uppala, S. M., Kallberg, P. W., Simmons, A. J., et al.: The ERA-40 re-analysis, Q. J. Roy. Meteor. Soc., 131, 2961–3012, doi:10.1256/qj.04.176, 2005. 7552

Vehkamäki, H., Kulmala, M., Napari, I., Lehtinen, K. E. J., Timmreck, C., Noppel, M., and Laaksonen, A.: An improved parameterization for sulfuric acid water nucleation rates for tropospheric and stratospheric conditions, J. Geophys. Res., 107, 4622, doi:10.1029/2002JD002184, 2002. 7553, 7554, 7585, 7587, 7595

Title Page

Abstract | Introduction

Conclusions | References

Tables | Figures

◄◄ | ►►

◄ | ►

Back | Close

Full Screen / Esc

Printer-friendly Version

Interactive Discussion

Verheggen, B., Cozic, J., Weingartner, E., Bower, K., Mertes, S., Connolly, P., Gallagher, M., Flynn, M., Choularton, T., and Baltensperger, U.: Aerosol partitioning between the interstitial and the condensed phase in mixed-phase clouds, J. Geophys. Res., 112, D23202, doi:10.1029/2007JD008714, 2007. 7560, 7585

5 Vignati, E., Wilson, J., and Stier, P.: M7: An efficient size-resolved aerosol microphysics module for large-scale aerosol transport models, J. Geophys. Res., 109, D22202, doi:10.1029/2003JD004485, 2004. 7547, 7550, 7551, 7553

Wilson, J., Cuvelier, C., and Raes, F.: A modeling study of global mixed aerosol fields, J. Geophys. Res., 106, 34081–34108, doi:10.1029/2000JD000198, 2001. 7547

10 Zdanovskii, A. B.: New methods for calculating solubilities of electrolytes in multicomponent systems, Zhur. Fiz. Khim., 22, 1475–1485, 1948. 7557, 7585

Zeleznik, F. J.: Thermodynamic properties of the aqueous sulfuric acid system to 350 K, J. Phys. Chem. Ref. Data, 20, 1157–1200, doi:10.1063/1.555899, 1991. 7557, 7585

Zhang, K., Wan, H., Wang, B., Zhang, M., Feichter, J., and Liu, X.: Tropospheric aerosol size

15   distributions simulated by three online global aerosol models using the M7 microphysics module, Atmos. Chem. Phys., 10, 6409–6434, doi:10.5194/acp-10-6409-2010, 2010. 7548, 7558

Zhang, K., Feichter, J., Kazil, J., Wan, H., Zhuo, W., Griffiths, A. D., Sartorius, H., Zahorowski, W., Ramonet, M., Schmidt, M., Yver, C., Neubert, R. E. M., and Brunke, E.-G.: Radon activ-

20   ity in the lower troposphere and its impact on ionization rate: a global estimate using different radon emissions, Atmos. Chem. Phys., 11, 7817–7838, doi:10.5194/acp-11-7817-2011, 2011. 7572

Title Page

Abstract | Introduction

Conclusions | References

Tables | Figures

◄ | ►

◄ | ►

Back | Close

Full Screen / Esc

Printer-friendly Version

Interactive Discussion

Table 1. An overview of the main differences between HAM1 and HAM2 in model configuration.

	HAM1 and HAM2 shared features	HAM1 specifics	HAM2 specifics
Atmospheric dynamics and physics	ECHAM5 (Roeckner et al., 2003, 2006a)	Stratiform cloud microphysics scheme by Lohmann and Roeckner (1996); Solar radiation scheme with four bands (Fouquart and Bonnel, 1980).	Two-moment stratiform cloud microphysics scheme by Lohmann et al. (2007); Solar radiation scheme extended to six bands (Cagnazzo et al., 2007).
Sulfuric acid gas	Sources and sinks include transport, chemical production, condensation, and aerosol nucleation.	Concentration equation is solved with three-step sequential operator splitting using explicit time stepping scheme; No distinction between cloudy and cloud-free parts of a model grid box.	Concentration equation is solved by a two-step operator splitting scheme with analytical solution for production and condensation (Kokkola et al., 2009); Complete removal of sulfuric acid gas from the air is assumed in the cloudy part of a model grid box (Kazil et al., 2010).
Aerosol nucleation	Vehkamäki et al. (2002) or Kulmala et al. (1998)	Vehkamäki et al. (2002) as default	New scheme by Kazil et al. (2010) as default, with optional H_2SO_4-organic nucleation based on the kinetic nucleation theory (Kuang et al., 2008) or cluster activation (Kulmala et al., 2006; Riipinen et al., 2007; Kazil et al., 2010). Old schemes by Vehkamäki et al. (2002) and by Kulmala et al. (1998) are still optional.
Aerosol water uptake	Dependent on the chemical compositions of aerosol particles and ambient relative humidity (with respect to water).	Considered only for non-organic aerosols, based on Zeleznik (1991), Zdanovskii (1948) and Stokes and Robinson (1966)	Considered for non-organic and organic aerosols, based on the κ-Köhler theory (Petters and Kreidenweis, 2007; O'Donnell et al., 2011).
Secondary organic aerosol (SOA)	Refractive indices of SOA are assumed the same as those of POA.	SOA is approximated as 15% of monoterpene emissions at surface (Dentener et al., 2006) and is assumed to condense immediately on existing aerosol particles and to have identical properties to primary organic aerosols (Stier et al., 2005).	The lifecycle of SOA is explicitly simulated; Emissions of biogenic precursors are computed interactively; Anthropogenic precursor emissions are prescribed (O'Donnell et al., 2011).
Sea salt emission	Interactive calculation based on Monahan et al. (1986) and Smith and Harrison (1998)	Smooth merging of emission functions in the particle radius range of 2–4 µm (Stier et al., 2005)	Monahan et al. (1986) formula for the radius range of 2–4 µm (see Sect. 4.4).
Dust emission	Interactive calculation using the Tegen et al. (2002) scheme		East Asia soil properties updated by Cheng et al. (2008).
In-cloud scavenging of aerosols	Prescribed scavenging parameter for each aerosol mode and cloud type (Stier et al., 2005).	Scavenging parameters are prescribed for three ambient temperature ranges (liquid cloud: $T > 273$ K, mixed-phase cloud: 238 K$< T < 273$ K, and ice cloud: $T < 238$ K).	Option to use temperature dependent scavenging parameters for mixed-phase stratiform clouds based on a relationship from (Verheggen et al., 2007).
Below-cloud scavenging of aerosols	Considered separately for rain and snow	Prescribed, mode dependent impaction scavenging coefficients for rain; One fixed coefficient for snow (Stier et al., 2005)	Optional scheme by Croft et al. (2009): Impaction scavenging coefficients for rain depend on the size distributions of aerosols and collectors; The coefficients for snow depend on aerosol size.

Title Page

Abstract | Introduction

Conclusions | References

Tables | Figures

◀◀ | ▶▶

◀ | ▶

Back | Close

Full Screen / Esc

Printer-friendly Version

Interactive Discussion

Table 2. List of simulations presented in this paper.

Simulation	Description	Section number
HAM1	ECHAM-HAM version 1 as described by (Stier et al., 2005)	4.1–4.7, 5.1–5.5
HAM2	Default configuration of ECHAM-HAM version 2 (this work)	4.1–4.7, 5.1–5.5
HAM2_H2SO4	Same as HAM2 but with the old treatment for the sulfuric acid gas equation	4.1
HAM2_NUL	Same as HAM2 but with the old nucleation scheme and numerics for the sulfric acid equation.	4.1
HAM2_cluster	Same as HAM2 but with cluster activation nucleation in the forested boundary layer	4.1, 5.3
HAM2_kinetic	Same as HAM2 but with kinetic nucleation in the forested boundary layer	4.1, 5.3
HAM2_OA	Same as HAM2 but with the old treatment with organic aerosol	4.2
HAM2_WAT	Same as HAM2 but with the old water-uptake scheme	4.3
HAM2_SS	Same as HAM2 but with the old sea salt emission scheme	4.4
HAM2_DU	Same as HAM2 but with the old dust emission scheme	4.5
HAM2_BLCLD	Same as HAM2 but with the below-cloud wet scavenging scheme proposed by Croft et al. (2009)	4.6
HAM2_INCLD	Same as HAM2 but with the modified in-cloud wet scavenging scheme for mixed-phase cloud	4.6
HAM2_INBLCLD	Same as HAM2 but with the modified in-cloud wet scavenging scheme for mixed-phase cloud *and* below-cloud wet scavenging scheme proposed by Croft et al. (2009)	4.6
HAM2_CLD	Same as HAM2 but with the Lohmann and Roeckner (1996) cloud microphysics without aerosol-cloud interaction	4.7

Table 3. Binary aerosol nucleation schemes available in ECHAM-HAM2 and their valid range of thermodynamical conditions. Boundary values are used in case the actual atmospheric condition is out of range.

	Temperature	Relative Humidity	H_2SO_4 Concentration	Note
Kulmala et al. (1998)	233–298 K	10–100 %	(No constraint)	
Vehkamäki et al. (2002)	230.15–305.15 K	0.01–100 %	$10^4\,cm^{-3}$–$10^{11}\,cm^{-3}$	HAM1 default
Kazil et al. (2010)	180–320 K	1–101 %	$10^5\,cm^{-3}$–$5 \times 10^9\,cm^{-3}$	HAM2 default

Table 4. Values of the hygroscopicity parameter κ used in ECHAM-HAM2 for the κ-Köhler theory based water uptake scheme. The observed ranges of κ listed in the rightmost column are quoted from Table 1 in Petters and Kreidenweis (2007), which were derived from the laboratory measured growth factor of particle radius. For primary organic aerosols, the observed range is obtained from mean κ values of various organic compounds other than secondary organic aerosol.

Species	κ	Observed Range of κ
Sulfate	0.60	0.33–0.72
Sea salt	1.12	0.91–1.33
Primary organic aerosol	0.06	0.006–0.44
Secondary organic aerosol	0.037	0.022–0.070
Black carbon	0	–
Mineral dust	0	–

Table 5. Annual mean global mass budget of SU, BC, POM, SS and DU simulated by two version of the HAM model and their relative differences. To put the numbers in perspective, the multi-model mean and standard deviation of the AeroCom intercomparison project (from Textor et al., 2006) are also listed. The standard deviations are given as percentages of the corresponding mean values. The AeroCom dry deposition listed here is the sum of dry deposition and sedimentation. For sea salt there is one outlier model which features very high emissions. We therefore cite the multi-model median (indicated by asterisks) instead of mean for the sea salt budget.

	HAM1	HAM2	HAM2 vs HAM1 Relative Diff.	AeroCom (Textor et al., 2006)	
				Mean	Std. Dev.
SO_4^{2-} particle					
Burden (Tg S)	0.78	0.85	+9 %	0.67	25 %
Sources (Tg S yr^{-1})					
Total	77.6	70.9	−8.6 %	59.7	22 %
Primary emissions	2.3	2.3	0.0 %		
Nucleation	0.11	0.21	+91 %		
H_2SO_4 condensation	27.1	25.8	−4.8 %		
Aqueous oxidation	48.0	42.5	−11 %		
Sinks (Tg S yr^{-1})					
Total	77.3	70.5	−8.8 %		
Dry deposition	2.16	2.33	+7.9 %	} 6.9	55 %
Sedimentation	1.62	1.56	−3.7 %		
Wet deposition	73.5	66.6	−9.4 %	52.8	22 %
Lifetime (days)	3.7	4.4	+16 %	4.12	18 %
Black carbon					
Burden (Tg)	0.11	0.13	+18 %	0.24	42 %
Sources (Tg yr^{-1})					
Emissions	7.7	7.7	0.0 %	11.9	23 %
Sinks (Tg yr^{-1})					
Dry deposition	0.59	0.64	+8.5 %	} 2.55	55 %
Sedimentation	0.02	0.02	0.0 %		
Wet deposition	7.19	7.14	−7.0 %	9.35	31 %
Lifetime (days)	5.3	5.9	+11 %	7.12	33 %
Aging time (days)	0.72	0.86	+19 %		

Title Page

Abstract | Introduction

Conclusions | References

Tables | Figures

◄ | ►

◄ | ►

Back | Close

Full Screen / Esc

Printer-friendly Version

Interactive Discussion

Table 5. Continued.

	HAM1	HAM2	HAM2 vs HAM1 Relative Diff.	AeroCom (Textor et al., 2006)	
				Mean	Std. Dev.
POM	POA + SOA	POA, SOA			
Burden (Tg)	0.99	0.83, 0.65	+49 % (POA+SOA)	1.70	27 %
Sources (Tg yr^{-1})					
Total	66.1	68.4	+3.5 % (POA+SOA)	96.6	26 %
POA emissions	47.0	47.1, –	+0.2 % (POA)		
SOA from monoterpenes	19.1	– , 3.7			
SOA from isoprene	–	– , 12.0			
Anthropogenic SOA emissions	–	– , 5.6			
Sinks (Tg yr^{-1})					
Dry deposition	4.9	3.3, 1.2	−8.2 % (POA+SOA)	} 19.2	49 %
Sedimentation	0.19	0.13, 0.06	0.0 % (POA+SOA)		
Wet deposition	61.4	43.9, 19.4	+3.1 % (POA+SOA)	76.7	32 %
Lifetime (days)	5.5	6.4 , 11.4	+16 % (POA), +107 % (SOA)	6.54	27 %
Aging time (days)	0.96	1.00, –	+4.2 % (POA)		
Sea salt					
Burden (Tg)	10.3	11.6	+13 %	6.37*	54 %
Sources (Tg yr^{-1})					
Emissions	5019	6110	+22 %	6280*	199 %
Sinks (Tg yr^{-1})					
Dry deposition	948	1484	+57 %	} 4377	219 %
Sedimentation	1376	2038	+48 %		
Wet deposition	2721	2591	−4.8 %	1902*	77 %
Lifetime (days)	0.75	0.69	−8.0 %	0.41*	58 %
Dust					
Burden (Tg)	10.3	11.6	+13 %	19.20	40 %
Sources (Tg yr^{-1})					
Emissions	751	805	+7.2 %	1840	49 %
Sinks (Tg yr^{-1})					
Dry deposition	44.8	56.1	+25 %	} 1235	84 %
Sedimentation	289	341	+18 %		
Wet deposition	423	410	−3.1 %	607	54 %
Lifetime (days)	5.0	5.2	+4 %	4.1	43 %
Aging time (days)	4.8	5.4	+12 %		

Title Page

Abstract | Introduction

Conclusions | References

Tables | Figures

◄◄ | ►►

◄ | ►

Back | Close

Full Screen / Esc

Printer-friendly Version

Interactive Discussion

Table 6. Impact of cloud microphysics parameterization on aerosol lifetime (unit: day). The sensitivity experiment HAM2_CLD uses the scheme of Lohmann and Roeckner (1996), while the standard ECHAM-HAM2 model uses the scheme of Lohmann et al. (2007). See Sects. 4.7 and 5.1 for further details.

	Aerosol lifetime		
	HAM2_CLD	HAM2	Relative diff.
SO_4^{2-} particle	3.6	4.4	+22 %
SOA	5.5	11.4	+107 %
Sea salt	0.59	0.69	+17 %
Black carbon	5.2	5.9	+13 %
POA	5.9	6.4	+8.5 %
Dust	5.0	5.2	+4.0 %

Table A1. List of observational data used in Sect. 5.2 for evaluating the simulated concentration of condensation nuclei. The measurements campaigns include: ACE-1 (Southern Hemisphere Marine Aerosol Characterization Experiment), ACE-ASIA (Asian Pacific Regional Aerosol Characterization Experiment), ARCTAS (Research of the Composition of the Troposphere from Aircraft and Satellites), INDOEX (Indian Ocean Experiment), INTEX-A (Intercontinental Chemical Transport Experiment – Phase A), INTEX-B (Intercontinental Chemical Transport Experiment – Phase B), ITOP (International Transport of Ozone and Precursors), PACDEX (PACific Dust EXperiment), RICO (Rain in Cumulus Over the Ocean), VOCALS (VAMOS Ocean Cloud Atmosphere Land Study), PASE (Pacific Atmospheric Sulfur Experiment), PEM-Tropics A (Pacific Exploratory Missions Tropics A), PEM-Tropics B (Pacific Exploratory Missions Tropics B), TRACE-P (TRansport and Chemical Evolution over the Pacific). The data are obtained from the NASA LaRC Airborne Science Data for Atmospheric Composition program (NASA LaRC), National Center for Atmospheric Research Earth Observing Laboratory (NCAR EOL), and the British Atmospheric Data Centre (BADC). The aircraft trajectories are shown in Fig. 9.

Field Campaign[1]	Platform	Latitude Range	Lontitude Range	Temporal coverage	Source
ACE-1	C-130	70° S–30° S	100° E–180° E	31 Oct–23 Dec 1991	NCAR EOL
ACE-ASIA	C-130	10° N–50° N	100° E–170° E	31 Mar–5 May 2001	NCAR EOL
ARCTAS	DC-8	32° N–90° N	169° W–37° W	3 Apr–22 Apr 2008 20 Jun–15 Jul 2008	NASA LaRC
ARCTAS	P3-B	32° N–81° N	164° W–69° W	1 Apr–21 Apr 2008 23 Jun–13 Jul 2008	NASA LaRC
INDOEX	C-130	10° S–17.5° N	65° E–85° E	16 Feb–24 Mar 1999	NCAR EOL
INTEX-A	DC-8	27° N–53° N	140° W–36° W	5 Aug–7 Sept 2007	NASA LaRC
INTEX-B	C-130	16° N–53° N	141° W–89° W	4 Mar–15 May 2006	NASA LaRC
	DC-8	16° N–53° N	175° E–86° W	5 Mar–16 May 2006	
ITOP	BAE-146	33° N–52° N	40° W–0° E	13 Jul–14 Aug 2004	BADC
MILAGRO	C-130	16° N–40° N	106° W–88° W	28 Feb–29 Mar 2006	NCAR EOL
PACDEX	HIAPER	20° N–60° N	136° E–105° W	29 Apr–25 May 2007	NCAR EOL
PASE	C-130	1° N–3° N	160° W–153° W	8 Aug–7 Sept 2007	NCAR EOL
PEM-Tropics A	DC-8	72° S–45° N	152° E–109° W	31 Aug–7 Oct 1996	NASA LaRC
	P3-B	35° S–39° N	165° W–77° W	16 Aug–27 Sep 1996	
PEM-Tropics B	DC-8	36° S–35° N	148° E–85° W	7 Mar–19 Apr 1999	NASA LaRC
	P3-B	21° S–40° N	166° W–76° W	12 Mar–12 Apr 1999	
RICO	C-130	15° N–21° N	72° W–57° W	24 Dec 2004–24 Jan 2005	NCAR EOL
TRACE-P	DC-8	13° N–46° N	113° E–118° W	27 Feb–10 Apr 2001	NASA LaRC
	P3-B	6° N–41° N	111° E–75° W	25 Feb–11 Apr 2001	
VOCALS	C-130	30° S–15° S	90° W–70° W	15 Oct–15 Nov 2008	NCAR EOL

Title Page

Abstract | Introduction

Conclusions | References

Tables | Figures

◀ | ▶

◀ | ▶

Back | Close

Full Screen / Esc

Printer-friendly Version

Interactive Discussion

**Table A2.** Aerosol optical depth (AOD, unitless) and aerosol radiative forcing (direct effect, unit: $W m^{-2}$) in simulations discussed in this paper. AOD_w and AOD_d stand for the optical depth associated with aerosol water and dry mass, respectively. The radiative forcing is presented in components: top-of-atmosphere clear-sky and all-sky shortwave forcing FSW_{clear}^{TOA} and FSW_{all}^{TOA}; surface clear-sky and all-sky shortwave forcing FSW_{clear}^{SFC} and FSW_{all}^{SFC}; top-of-atmosphere clear-sky and all-sky longwave forcing FLW_{clear}^{TOA} and FLW_{all}^{TOA}, surface clear-sky and all-sky longwave forcing FLW_{clear}^{SFC} and FLW_{all}^{SFC}. Numbers given in bold are the larges and smallest values among the sensitivity experiments carried out with HAM2.

	AOD	AOD_w	AOD_d	FSW_{clear}^{TOA}	FSW_{all}^{TOA}	FSW_{clear}^{SFC}	FSW_{all}^{SFC}	FLW_{clear}^{TOA}	FLW_{all}^{TOA}	FLW_{clear}^{SFC}	FLW_{all}^{SFC}
HAM2	0.135	0.094	0.041	−3.79	−1.96	−5.76	−3.81	0.32	0.20	1.32	0.78
HAM2_H2SO4	0.130	0.089	0.041	−3.69	−1.94	−5.71	−3.86	0.31	0.20	1.21	0.76
HAM2_NUL	0.137	0.096	0.041	−3.86	−1.98	−5.83	−3.83	0.33	0.20	1.32	0.78
HAM2_cluster	0.135	0.094	0.041	−3.80	−1.95	−5.76	−3.80	0.32	0.20	1.32	0.78
HAM2_kinetic	0.135	0.095	0.040	−3.81	−1.94	−5.77	−3.79	0.32	0.20	1.32	0.78
HAM2_WAT	**0.163**	**0.123**	0.041	**−4.33**	−2.03	**−6.31**	−3.89	**0.45**	**0.24**	**1.94**	**0.91**
HAM2_OA	0.131	0.089	0.042	−3.54	−1.85	−5.40	−3.59	0.30	0.19	1.31	0.78
HAM2_DU	0.134	0.094	0.040	−3.78	−1.95	−5.74	−3.80	0.32	0.20	1.31	0.78
HAM2_SS	0.139	0.098	0.041	−4.06	**−2.12**	−6.03	−3.97	0.34	0.21	1.45	0.85
HAM2_BLCLD	0.124	0.085	0.039	−3.52	−1.86	−5.42	−3.66	0.29	0.19	1.17	0.74
HAM2_INCLD	0.145	0.101	**0.044**	−4.08	−2.07	−6.20	**−4.09**	0.37	0.23	1.40	0.83
HAM2_INBLCLD	0.130	0.089	0.041	−3.69	−1.94	−5.71	−3.86	0.31	0.20	1.21	0.76
HAM2_CLD	**0.109**	**0.074**	**0.034**	−3.06	**−1.59**	**−4.72**	−3.14	**0.24**	**0.15**	**1.11**	**0.70**

	Nucleation Mode r < 0.005 μm σ = 1.59	Aitken Mode 0.005 μm < r < 0.05 μm σ = 1.59	Accumulation Mode 0.05 μm < r < 0.5 μm σ = 1.59	Coarse Mode r < 0.5 μm σ = 2.0
Soluble	SU	SU BC POA SOA_IS1 SOA_IS2 SOA_MO1 SOA_MO2 SOA_ANT	SU BC POA DU SS SOA_IS1 SOA_IS2 SOA_MO1 SOA_MO2 SOA_ANT	SU BC POA DU SS SOA_IS1 SOA_IS2 SOA_MO1 SOA_MO2 SOA_ANT
Insoluble		BC POA SOA_IS1 SOA_IS2 SOA_MO1 SOA_MO2 SOA_ANT	DU	DU

Fig. 1. Aerosol modes and compositions considered in HAM2. Adapted and updated from Table 1 in Stier et al. (2005). The chemical compositions include sulfate (SU), black carbon (BC), primary organic aerosol (POA), mineral dust (DU), sea salt (SS), and secondary organic aerosol (SOA). SOA is further divided into different products from isoprene oxidation (SOA_IS1 and SOA_IS2), from monoterpene oxidation (SOA_MO1 and SOA_MO2), and from the oxidation of anthropogenic precursors (SOA_ANT). As for the mode parameters, r stands for the number median radius, and σ the prescribed standard deviation.
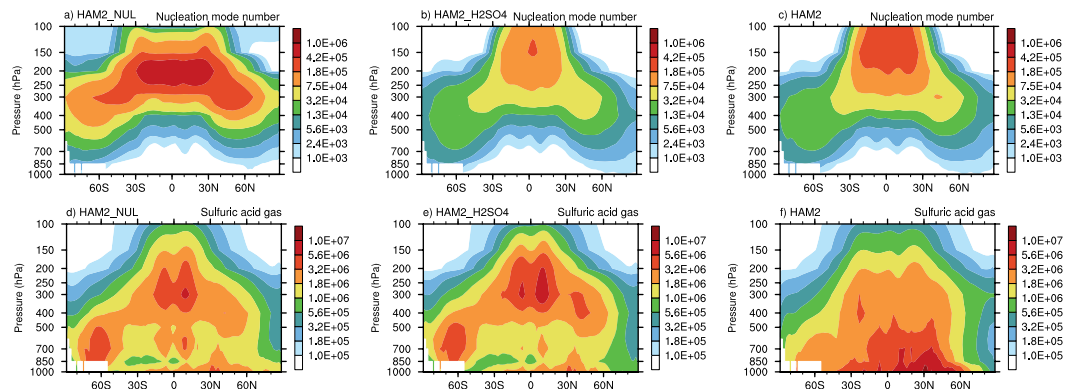
Fig. 2. and zonal mean vertical cross-sections of the number concentration of nucleation mode particles [upper row, unit: particles cm^{-3} STP (1013.25 hPa, 273.15 K)] and mass concentration of H_2SO_4 gas (lower row, unit: molecules cm^{-3}). The three columns correspond to different simulations, as indicated by the title of each panel: "HAM2" refers to the standard ECHAM-HAM2 configuration; "HAM2_H2SO4" uses the Kazil et al. (2010) nucleation scheme but the old handling of the H_2SO_4 equation (cf. Sect. 4.1); "HAM2_NUL" uses the Vehkamäki et al. (2002) parameterization and the old treatment of H_2SO_4. All other aspects of model configuration are identical in the three simulations.
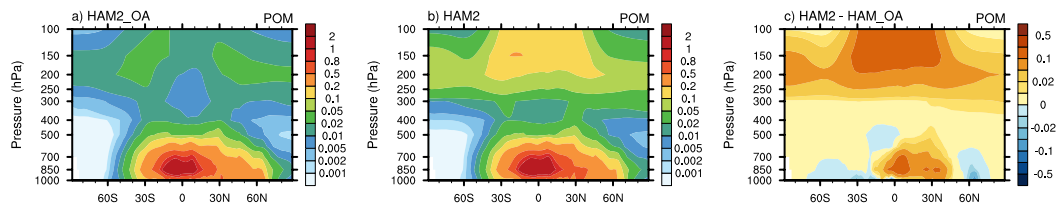
Fig. 3. Temporal and zonal mean vertical cross-sections of the mass concentration of particulate organic matter (POM) (unit: μg m^{-3}). The middle panel shows results from the standard ECHAM-HAM2 model (i.e., with the O'Donnell et al. (2011) SOA submodel switched on); The left panel corresponds to a sensitivity experiment HAM2_OA that uses the old (HAM1) simple SOA scheme (see Sect. 4.2 and Stier et al., 2005); The difference between the two simulations is indicated in panel **(c)**.
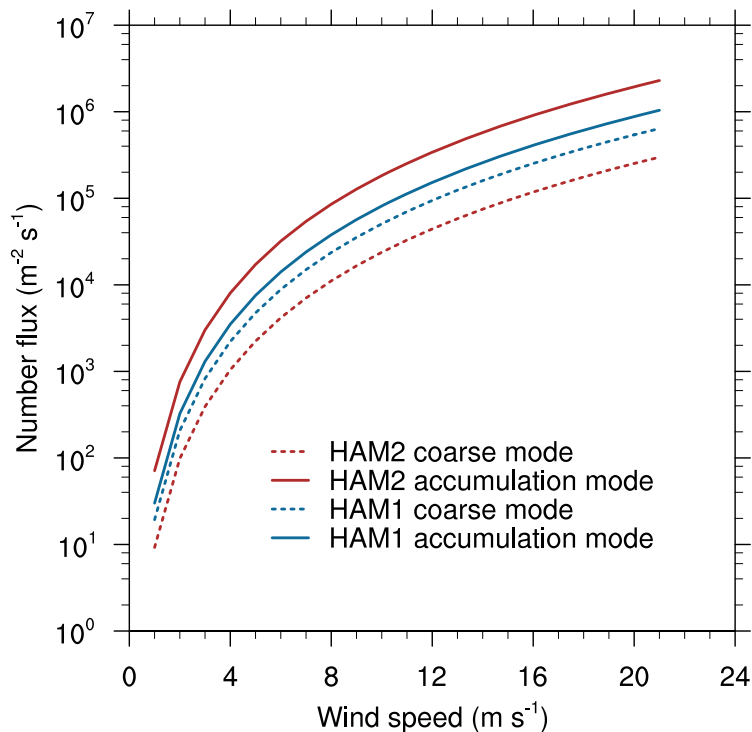
Fig. 4. Accumulation mode and coarse mode sea salt aerosol number fluxes (unit: $m^{-2}\,s^{-1}$) as functions of 10-m wind speed (unit: $m\,s^{-1}$), given by different implementations of the Monahan et al. (1986) and Smith and Harrison (1998) sea salt emission schemes. The blue curves correspond to the the old (HAM1) version, and red the new (HAM2) version.
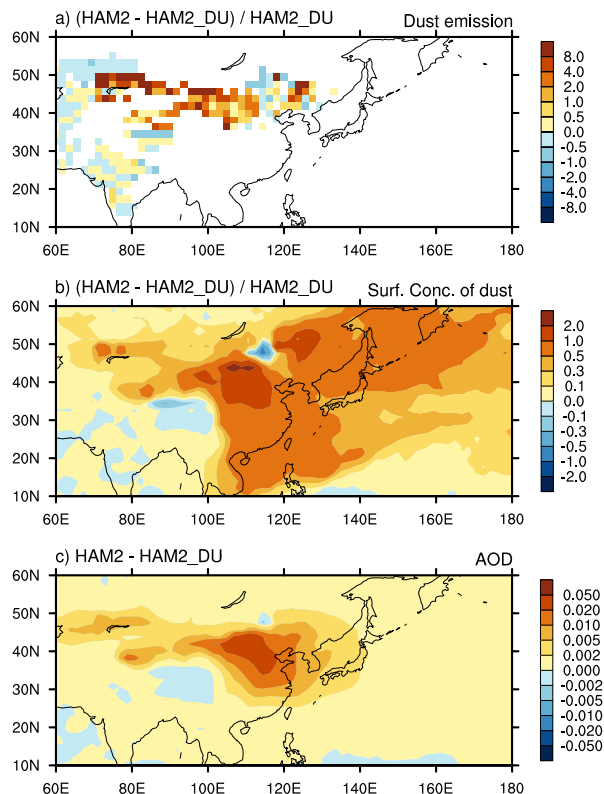
Fig. 5. (a) Relative changes in dust emission due to modified soil properties in East Asia, given as relative difference of annual mean mass flux; **(b)** corresponding relative changes in the mass concentration of dust aerosols in the lowest model layer; **(c)** the resulting changes in aerosol optical depth (AOD).

Title Page

Abstract | Introduction

Conclusions | References

Tables | Figures

Back | Close

Full Screen / Esc

Printer-friendly Version

Interactive Discussion
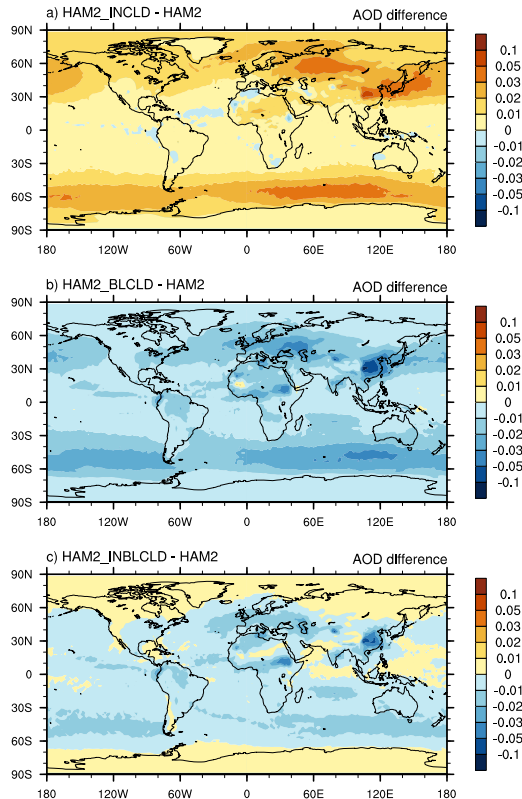
Fig. 6. **(a)** Changes in annual mean AOD caused by modification in the in-cloud scavenging of mixed-phase stratiform clouds; **(b)** Changes due to modifications by Croft et al. (2009) in the below-cloud (rain and snow) scavenging parameterization. **(c)** The combined effect of modified in-cloud and below-cloud scavenging. The four experiments shown here (HAM2, HAM2_INCLD, HAM2_BLCLD and HAM2_INBLCLD, cf. Table 2) are identical in all other aspects of model configuration. See Sect. 4.6 for further details.

Title Page

Abstract | Introduction

Conclusions | References

Tables | Figures

Back | Close

Full Screen / Esc

Printer-friendly Version

Interactive Discussion
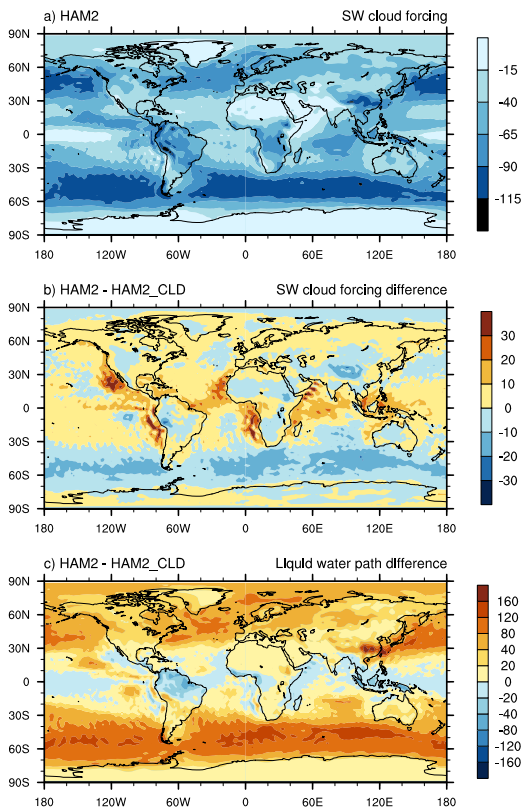
Fig. 7. (a) Annual mean shortwave cloud radiative forcing (W m^{-2}) simulated with the standard ECHAM-HAM2 model; **(b)** differences in shortwave cloud radiative forcing between HAM2 and a sensitivity experiment HAM2_CLD using the old cloud microphysics scheme (Lohmann and Roeckner, 1996) and without aerosol activation; **(c)** differences in annual mean liquid water path (g m^{-2}) between the two experiments. See Sect. 4.7 for further details.
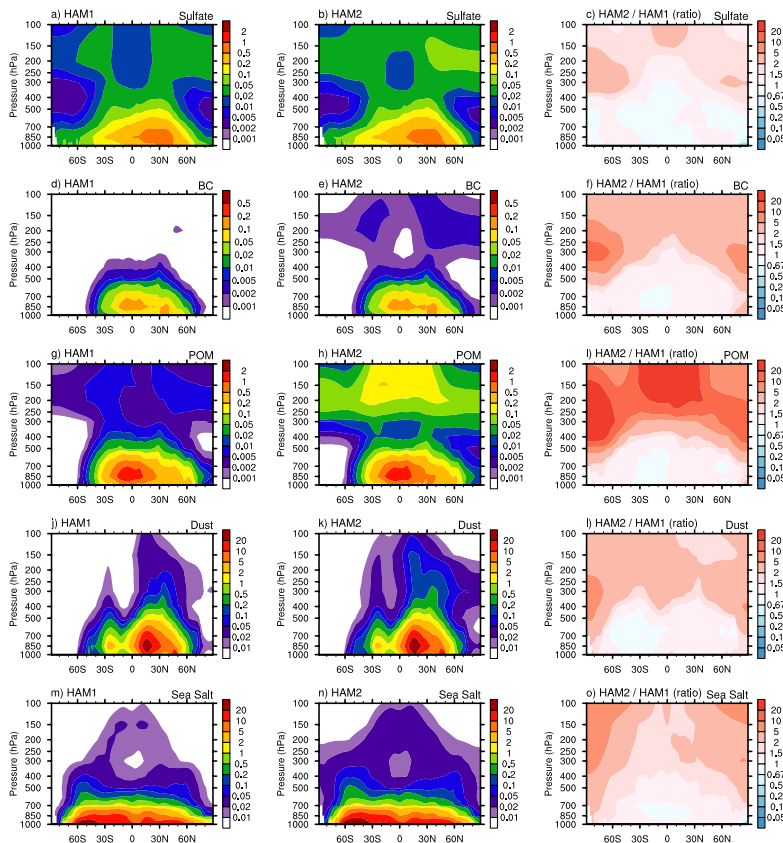
Fig. 8. Annual and zonal mean cross-sections of aerosol mass concentration (unit: µg m^{-3}) simulated by HAM1 (left column) and HAM2 (middle column), and the ratio (right column).

Full Screen / Esc

Printer-friendly Version

Interactive Discussion
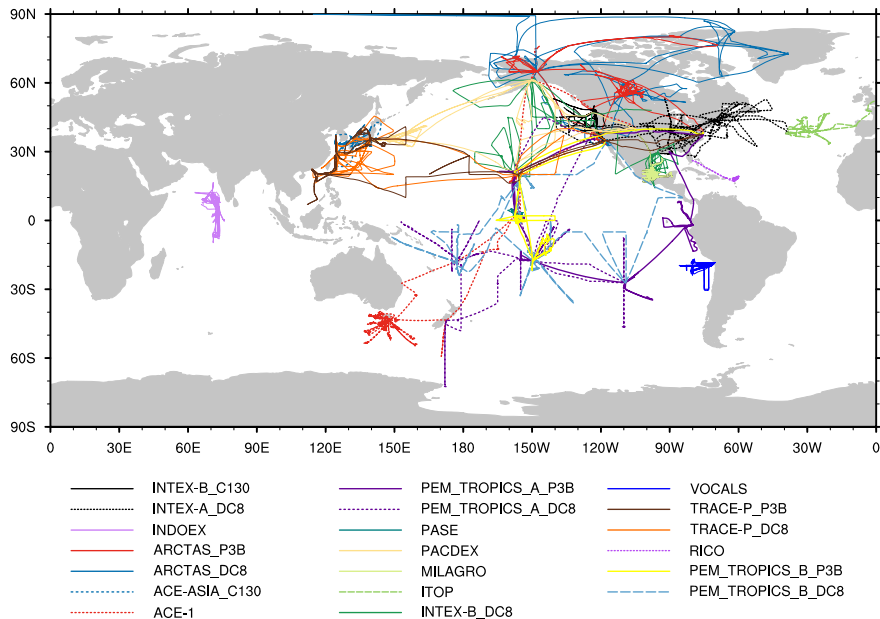
Fig. 9. Aircraft trajectories of the condensation nuclei measurements used for model evaluation in Sect. 5.2 and Figs. 10 and 11. Further details of the campaigns are listed in Table A1 of the Appendix.
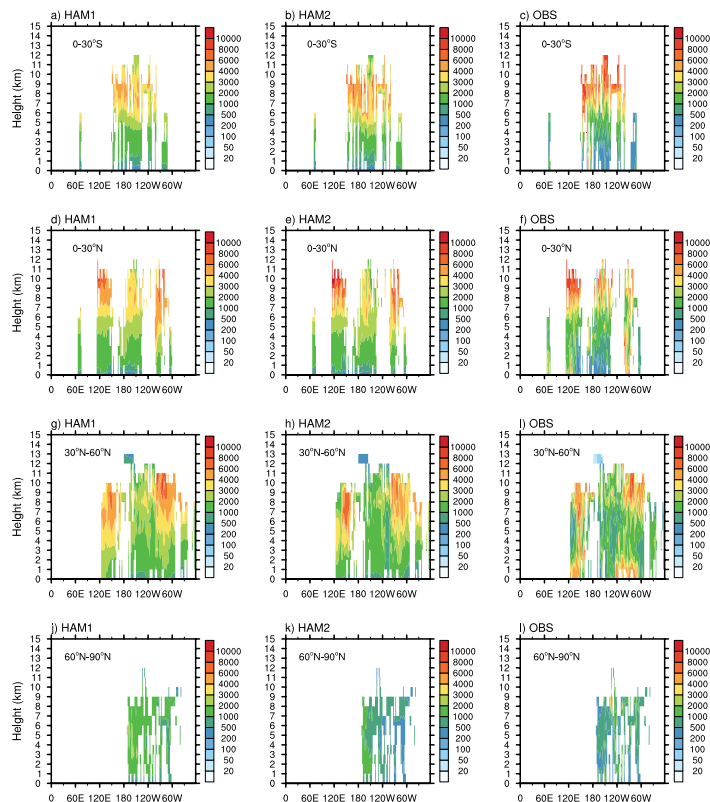
Fig. 10. Vertical distribution of simulated and observed condensation nuclei concentrations [unit: cm^{-3} STP (1013.25 hPa, 273.15 K)] in different regions. The observational data are compiled from campaign measurements shown in Table A1 and Fig. 9. Model results are derived from daily mean output of the months in which the measurements were obtained. Model CN concentration is calculated by integrating the simulated number size distribution above the lower cut-off dry diameter (0.01 µm). See Sect. 5.2 for further details.

Title Page

Abstract | Introduction

Conclusions | References

Tables | Figures

◀ | ▶|

◀ | ▶

Back | Close

Full Screen / Esc

Printer-friendly Version

Interactive Discussion
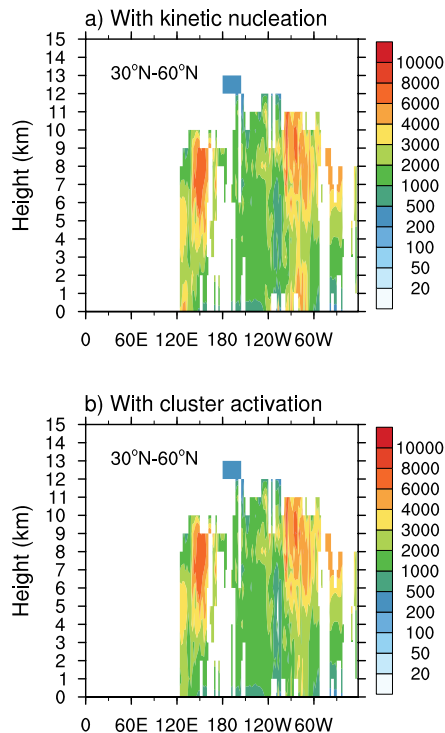
Fig. 11. Vertical distribution of condensation nuclei concentrations [unit: cm^{-3} STP (1013.25 hPa, 273.15 K)] in Northern Hemisphere midlatitudes, simulated by HAM2 with additional parameterization switched on in the planetary boundary layer to take into account the nucleation of H$_2$SO$_4$ and an organic compound. The upper panel uses the kinetic nucleation scheme of Kuang et al. (2008). The lower panel uses a cluster nucleation scheme (Kulmala et al., 2006; Riipinen et al., 2007; Kazil et al., 2010). See Sect. 5.2 for further details.
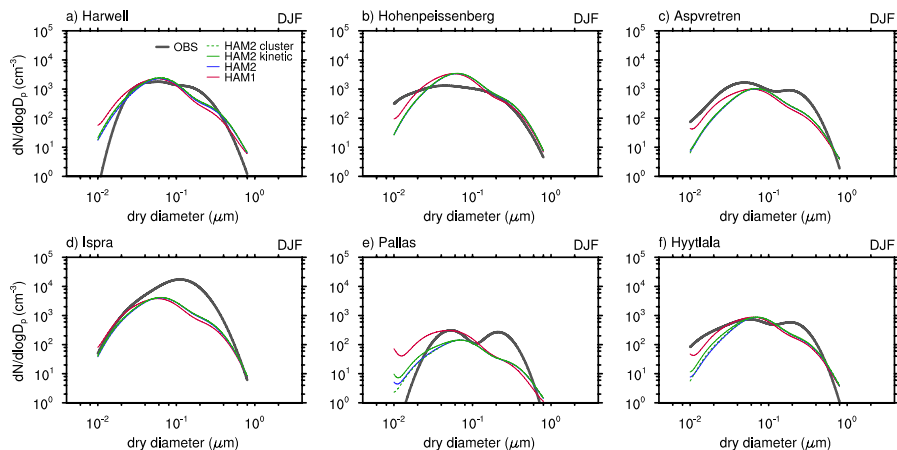
Fig. 12. Comparison of the simulated and measured aerosol size distributions in the planetary boundary layer over land in boreal winter (December-January-February). The thick black curves are the observed median size distributions from Putaud et al. (2003) and Tunved et al. (2003). Model results (the colored curves) are plotted only for the diameter range between 0.01 and 0.8 µm because this is the range measured in the references. Note that most parts of the dotted lines underlie solid color lines.
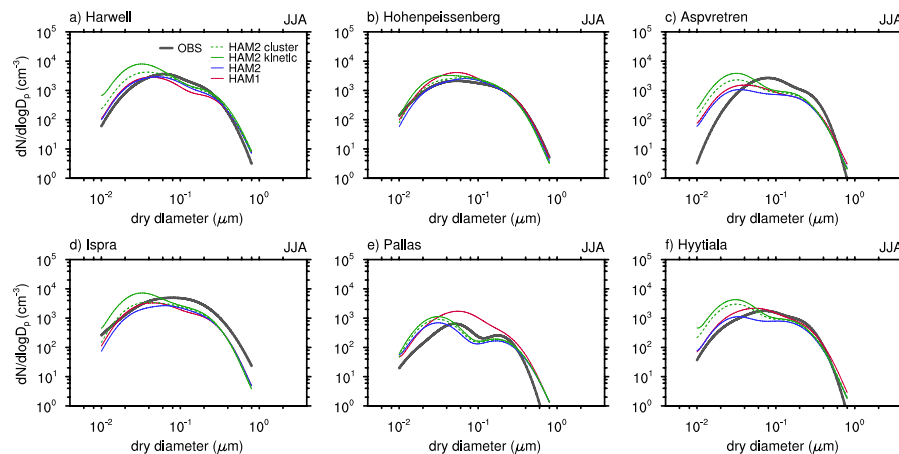
Fig. 13. As in Fig. 12 but for boreal summer (June-July-August).
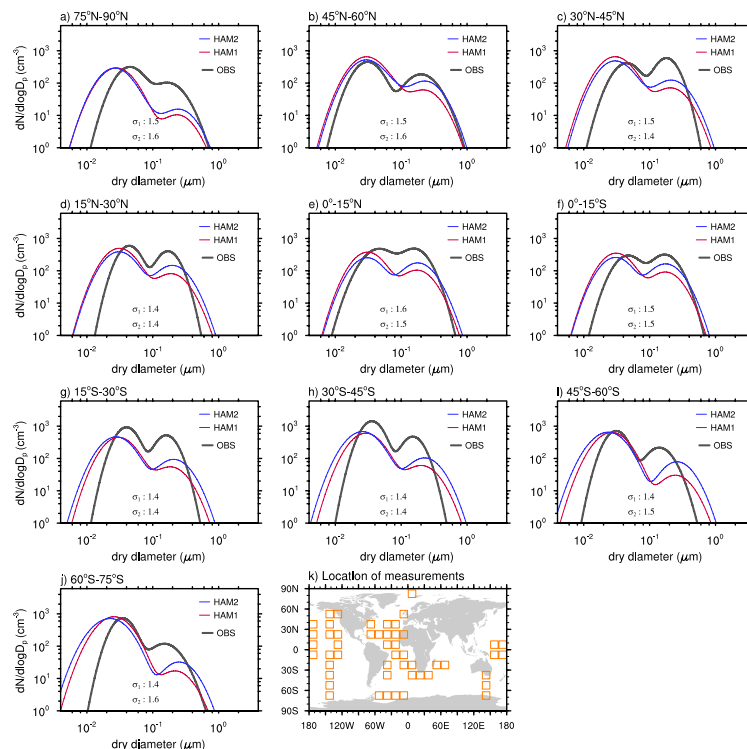
Fig. 14. Comparison of the measured (black curves) and simulated (colored curves) size distribution functions of the Aitken and accumulation modes (soluble and insoluble) in the marine boundary layer. The observations are a 30-yr climatology covering the brown boxes shown in panel **(k)**, compiled by Heintzenberg et al. (2000). The simulations shown in red and blue correspond to the HAM1 and HAM2 simulations, respectively. σ_1 and σ_2 in each panel are the observed standard deviation of the Aitken and accumulation mode. In the HAM model a fixed value of 1.59 is prescribed for both modes.

Title Page

Abstract | Introduction

Conclusions | References

Tables | Figures

◄ | ►

◄ | ►

Back | Close

Full Screen / Esc

Printer-friendly Version

Interactive Discussion
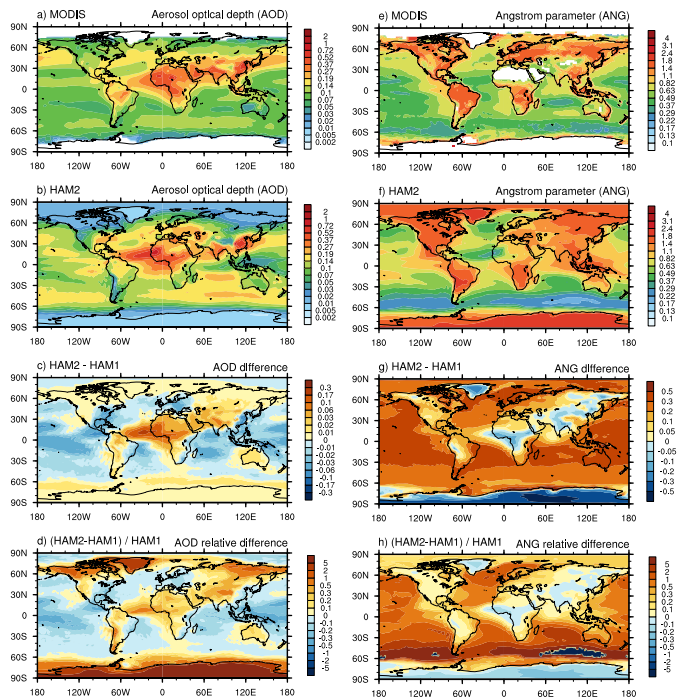
Fig. 15. Geographical distribution of the annual mean aerosol optical depth (AOD, left column) and Ångström parameter (ANG, right column) from the MODIS retrieval (top row), simulated by HAM2 (second row), and the differences between HAM2 and HAM1 results (third and bottom rows). The displayed satellite retrievals are multi-year mean fields. The AOD fields are calculated/retrieved at mid-visible wavelength 0.55 μm. The MODIS Ångström parameter is retrieved using the wavelengths 0.55 μm and 0.865 μm over the ocean, and 0.47 μm and 0.66 μm over land. The model-simulated ANG is calculated using the wavelengths 0.55 μm and 0.825 μm at all grid points.
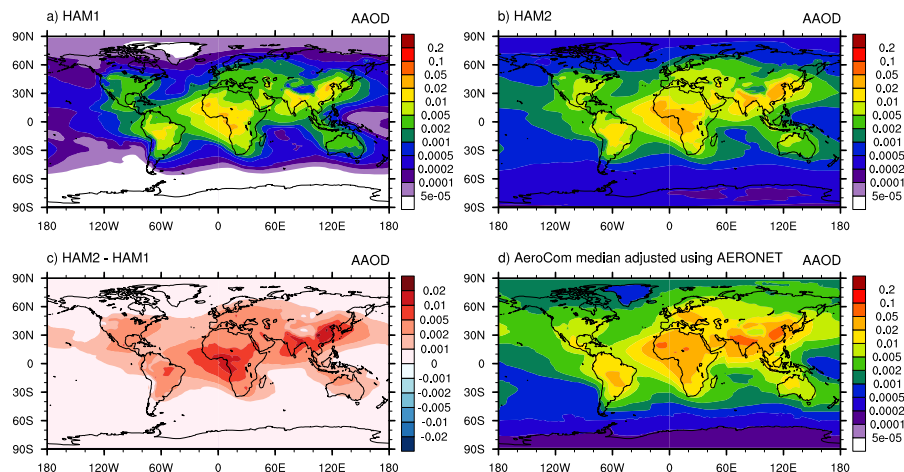
Fig. 16. Geographical distribution of the annual mean aerosol absorption optical depth (AAOD) simulated by HAM1 and HAM2 (top row), their differences (bottom left panel), and the reference result compiled by S. Kinne (bottom right panel) using the AeroCom multi-model median adjusted with AERONET measurements.
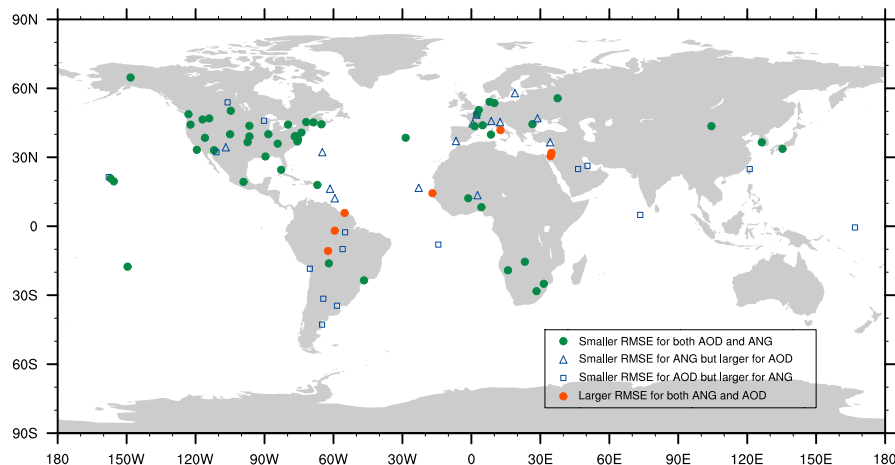
Fig. 17. Map showing the AERONET sites at which the daily mean aerosol optical depth (AOD) and Ångström parameter (ANG) of the year 2000 are used for the comparison in Fig. 18. At each site the root mean square error (RMSE, of daily mean AOD or ANG) against measurements is computed for both the HAM1 and HAM2 simulaitons. Green dots indicate improved results in HAM2 (reduced RMSE) for both AOD and ANG; Orange dots indicate degraded results for both parameters; Empty triangles and rectangles mark the locations where mixed results are obtained. See Sect. 5.4 for further details.
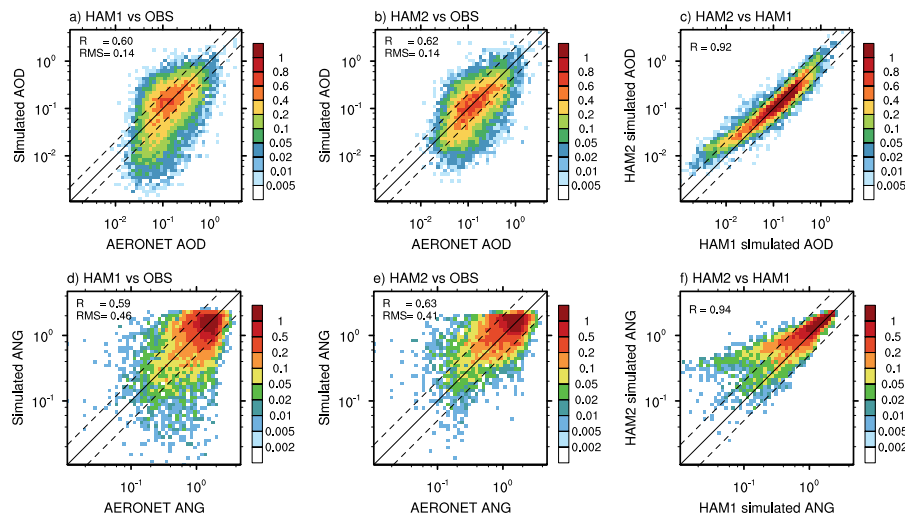
Fig. 18. Comparison of the AERONET-retrieved and model-simulated aerosol optical depth (upper row) and Ångström parameter (lower row). The color shading shows the joint probability density distribution (unit: %) as a function of, for example in panel **(a)**, the AERONET-retrieved and HAM1 simulated AOD, computed from the daily mean measurement retrieved from AERONET for the year 2000 at all locations indicated in Fig. 17 and model output (also daily means) sampled at the same time instances and locations. See Sect. 5.4 for further details. The R and RMS values noted in each panel are the correlation coefficient and root mean square difference of the two data series.

Full Screen / Esc

Printer-friendly Version

Interactive Discussion
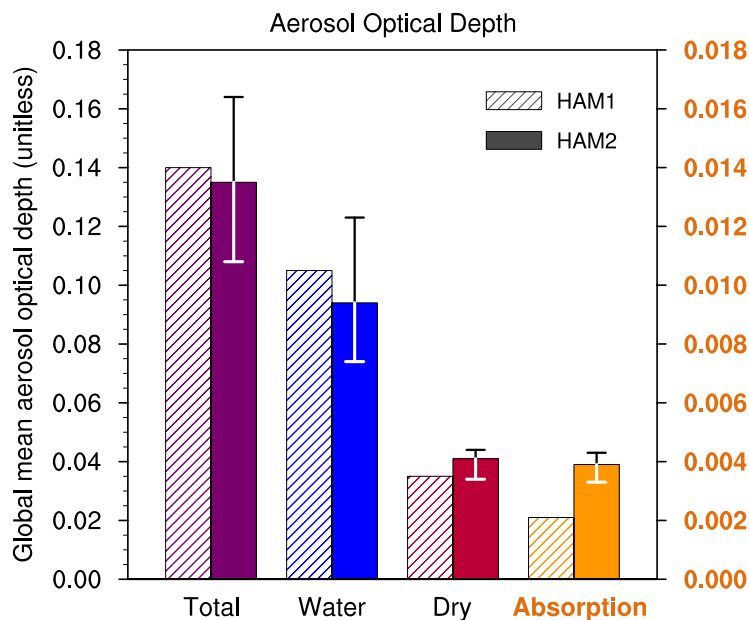
Fig. 19. Global and annual mean aerosol optical depth simulated by HAM1 and HAM2, the corresponding contributions from aerosol water and dry mass, as well as the absorption AOD. Whiskers associated with the HAM2 results indicate the ranges given by the sensitivity experiments listed in Table 2. Note that the absorption AOD is displayed with a different scale (see the y-axis on the right, in orange).
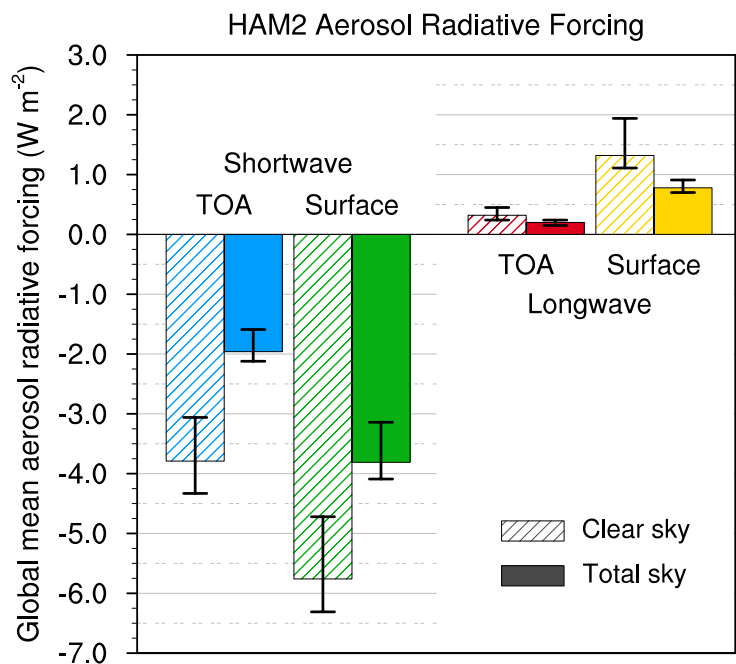
Fig. 20. Global and annual mean aerosol direct radiative effect simulated by HAM2 at top of the atmosphere (TOA) and at the Earth's surface. Whiskers indicate the spread among the HAM2 sensitivity experiments in Table 2.
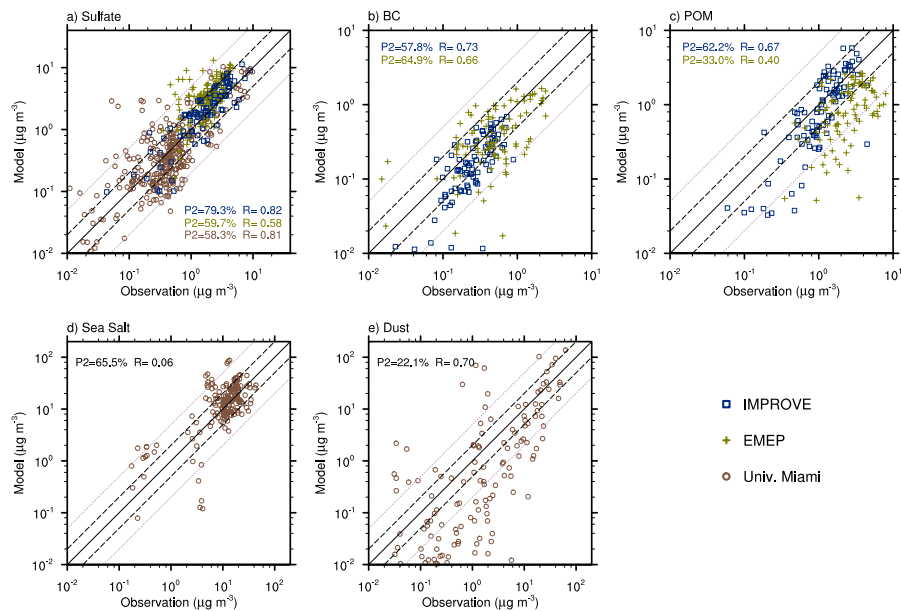
Fig. A1. Caption on next page.

Fig. A1. Scatter plot comparing the observed and HAM2-simulated monthly mean surface mass concentrations (unit: $\mu g\, m^{-3}$) of **(a)** sulfate, **(b)** black carbon, **(c)** particulate organic matter, **(d)** sea salt, and **(e)** dust. The solid lines indicate the 1:1 ratio. The dashed (and dotted) lines indicate domains in the diagram in which the simulated concentrations agree with the observations within a factor of 2 (and 5). Also shown in each panel are the percentage of samples in agreement within a factor of 2 (the P2 value), and the correlation coefficient between simulation and observation (the R-value). Blue squares indicate comparison with measurements collected in the IMPROVE network (http://vista.cira.colostate.edu/improve/), green crosses the EMEP network (http://www.emep.int), and brown circles the University of Miami network (data by courtesy of J. Prospero). Data from the University of Miami are multi-year monthly mean values from remote marine sites, while the IMPROVE and EMEP data are available as daily mean. When comparing the simulated concentrations with observations in the year 2000, the model-calculated daily mean values are sampled on the same days as the measurements and then averaged over each month. To increase the amount of measurements in the evaluation, we also use BC and POM data of the years 2002 and 2003 from EMEP. Considering that our simulations are nudged to the year 2000, the temporal sampling of daily model output according to measurement time is skipped in this case. The simulated monthly means are computed from all model time steps in the month. Furthermore, following Stier et al. (2005), in this comparison we have only included the stations at which the geopotential height of the lowest model layer is less than 200 m different from the actual altitude of the measurement, so as to ensure comparability.

Title Page

Abstract | Introduction

Conclusions | References

Tables | Figures

◄ | ►|

◄ | ►

Back | Close

Full Screen / Esc

Printer-friendly Version

Interactive Discussion